



**HAL**  
open science

## Eco-friendly gelatin films with rosin-grafted cellulose nanocrystals for antimicrobial packaging

Liliane S.F. Leite, Stanley Bilatto, Rafaella T. Paschoalin, Andrey C. Soares, Francys K.V. Moreira, Osvaldo N. Oliveira, Luiz H.C. Mattoso, Julien Bras

### ► To cite this version:

Liliane S.F. Leite, Stanley Bilatto, Rafaella T. Paschoalin, Andrey C. Soares, Francys K.V. Moreira, et al.. Eco-friendly gelatin films with rosin-grafted cellulose nanocrystals for antimicrobial packaging. *International Journal of Biological Macromolecules*, 2020, 165, pp.2974 - 2983. 10.1016/j.ijbiomac.2020.10.189 . hal-03492673

**HAL Id: hal-03492673**

**<https://hal.science/hal-03492673>**

Submitted on 7 Nov 2022

**HAL** is a multi-disciplinary open access archive for the deposit and dissemination of scientific research documents, whether they are published or not. The documents may come from teaching and research institutions in France or abroad, or from public or private research centers.

L'archive ouverte pluridisciplinaire **HAL**, est destinée au dépôt et à la diffusion de documents scientifiques de niveau recherche, publiés ou non, émanant des établissements d'enseignement et de recherche français ou étrangers, des laboratoires publics ou privés.



Distributed under a Creative Commons Attribution - NonCommercial 4.0 International License

# 1 Eco-friendly gelatin films with rosin-grafted cellulose 2 nanocrystals for antimicrobial packaging

3 *Liliane S. F. Leite<sup>a,b,c</sup>, Stanley Bilatto<sup>b</sup>, Rafaella T. Paschoalin<sup>c</sup>, Andrey C. Soares<sup>b</sup>, Francys K. V.*  
4 *Moreira<sup>d</sup>, Osvaldo N. Oliveira Jr.<sup>c</sup>, Luiz H. C. Mattoso<sup>a,b</sup>, Julien Bras<sup>e,f\*</sup>*

5 <sup>a</sup>Federal University of São Carlos, Graduate Program in Materials Science and Engineering  
6 (PPGCEM), 13565-905, São Carlos-Brazil, [lilianesamara@gmail.com](mailto:lilianesamara@gmail.com)

7 <sup>b</sup>National Nanotechnology Laboratory for Agribusiness, Embrapa Instrumentação, XV de  
8 Novembro street, 1452, 13560-979, São Carlos-Brazil, [stanleyebr@gmail.com](mailto:stanleyebr@gmail.com),  
9 [andreycoatrini@gmail.com](mailto:andreycoatrini@gmail.com) [luiz.mattoso@embrapa.br](mailto:luiz.mattoso@embrapa.br)

10 <sup>c</sup>University of São Paulo, São Carlos Institute of Physics, 13560-970, São Carlos-Brazil,  
11 [rafa.r RTP@gmail.com](mailto:rafa.r RTP@gmail.com), [chu@ifsc.usp.br](mailto:chu@ifsc.usp.br)

12 <sup>d</sup>Department of Materials Engineering, Federal University of São Carlos, Rod. Washington Luis,  
13 km 235, São Carlos (SP), 13565-905, Brazil. [moreira.fkv@dema.ufscar.br](mailto:moreira.fkv@dema.ufscar.br)

14 <sup>e</sup>University Grenoble Alpes, CNRS, Grenoble INP, LGP2, F-38400 Grenoble, France,

15 <sup>f</sup>Nestle Research Center, 1000 Lausanne, Switzerland

16

17 KEYWORDS. Gelatin; rosin; cellulose nanocrystal; antimicrobial properties; food packaging.

18

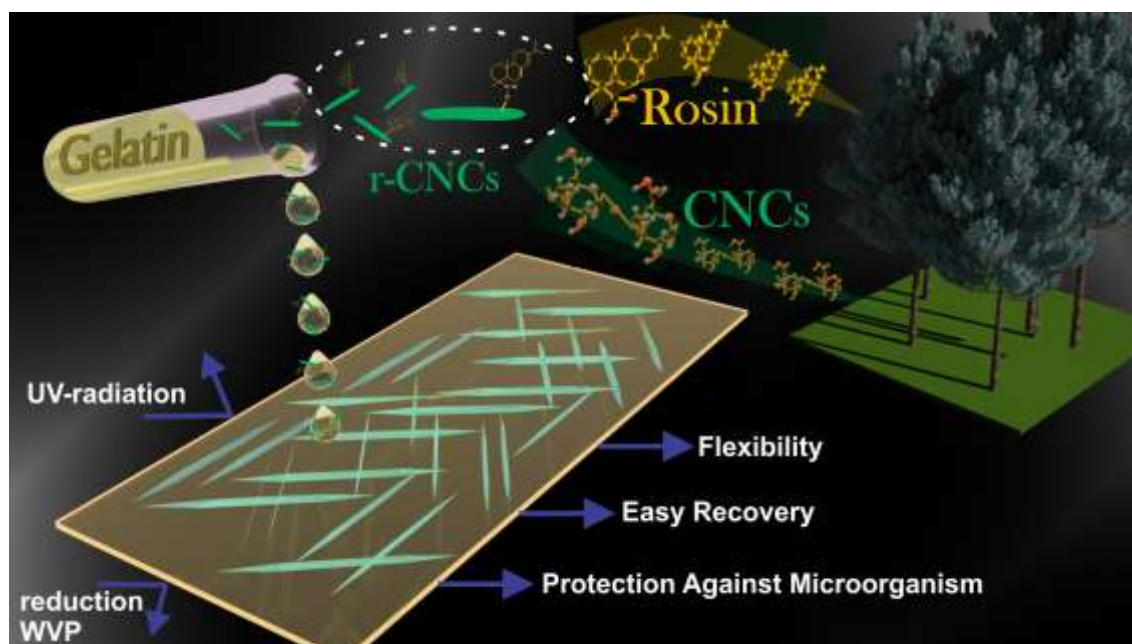
19

20

21 ABSTRACT

22 We report on gelatin films incorporating rosin-grafted cellulose nanocrystals (r-CNCs), which fulfill  
23 the most relevant requirements for antimicrobial packaging applications. Transparent gelatin/r-  
24 CNCs bionanocomposite films (0.5 – 6 wt% r-CNCs) were obtained by solution casting and  
25 displayed high UV-barrier properties, which were superior to the most used plastic packaging films.  
26 The gelatin/r-CNCs films exhibited a moderate water vapor permeability (0.09 g mm/m<sup>2</sup> h kPa),  
27 and high tensile strength (40 MPa) and Young's modulus (1.9 GPa). The r-CNCs were more  
28 efficient in improving the optical, water vapor barrier and tensile properties of gelatin films than  
29 conventional CNCs. Grafting of rosin on CNCs resulted in an antimicrobial nanocellulose that  
30 inhibited the growth of *Staphylococcus aureus* and *Escherichia coli*. The antibacterial properties of  
31 r-CNCs were sustained in the gelatin films, as demonstrated by agar diffusion tests and proof-of-  
32 principle experiments involving cheese storage. Overall, the incorporation of r-CNCs as active  
33 fillers in gelatin films is a suitable approach for producing novel eco-friendly, antimicrobial  
34 packaging materials.

35 GRAPHICAL ABSTRACT



36  
37

38 1. INTRODUCTION

39 Sustainability related to food plastic packaging has worldwide relevance owing to the need  
40 for safe disposal of post-consumer plastic wastes [1]. These problems can be mitigated if natural  
41 biodegradable polymers are employed as a packaging material, for which biopolymers have to  
42 exhibit suitable physical properties and increase the quality and safety of foods [2,3]. Desirable

43 properties of a packaging material include adequate mechanical strength, thermal stability,  
44 recyclability, biodegradability, and barrier against water vapor and oxygen [4]. Research has been  
45 focused on incorporating antimicrobial agents in packaging films to delay microbial growth [5],  
46 which is the major cause of deterioration of foods [6]. This microbial growth may cause off-flavor  
47 development, textural changes, loss of nutritive value, shelf-life reduction, increased risk of  
48 foodborne illnesses [7], thus rendering the product unacceptable for human consumption [8].

49 Proteins such as gelatin can be suitable for food packaging due to their renewability,  
50 biodegradability, low cost, film-forming ability, and edible nature [1,9,10]. Gelatin is a water-  
51 soluble protein produced from partial hydrolysis of collagen, one of the most used biopolymers in  
52 the food and pharmaceutical fields [11]. Gelatin films have suitable properties, such as  
53 transparency, biodegradability, and low oxygen permeability [12], but they show poor barrier  
54 properties against moisture and only moderate mechanical strength under high relative humidity  
55 [13]. These drawbacks could be overcome by incorporating reinforcing nanoparticles, such as  
56 cellulose nanocrystals (CNCs), in gelatin films [9,16–19]. CNCs are biodegradable, renewable, and  
57 exhibit a low density, high elastic modulus (~150 GPa), and tensile strength (~7.5 GPa), being  
58 produced in a commercial scale [20]. In addition to their use in polymer nanocomposites [21] to  
59 enhance the physical properties of protein films [22–25], CNCs can also be chemically modified to  
60 possess functionalities [26–29] such as antibacterial activity as with incorporation of titanium oxide  
61 [30] and silver [31]. A limitation of this latter approach, however, is the toxicity of these metals that  
62 could be released to the food [32]. This is motivation for the use of natural antimicrobial agents.

63 Rosin is an abundant natural product of pine resins, which is produced in more than 1  
64 million tons annually [33,34] and contains a mixture of acids (ca. 90%) with hydrogenated  
65 phenanthrene ring structures [35]. These acids are used in such applications as renewable feedstocks  
66 for polymer synthesis due to their biodegradability and nontoxicity [33,34,36]. CNCs grafted with  
67 natural rosin mixtures (r-CNCs) showed antimicrobial activity against Gram-negative and Gram-

68 positive bacteria [37]. Rosin-based bionanocomposites have been tested in active packaging films  
69 [38,39], but their preparation required chloroform or dichloromethane to disperse the polymer,  
70 limiting their application in the food industry.

71       Herein, rosin-grafted CNCs were synthesized and incorporated in gelatin films to enhance  
72 their physical properties for antimicrobial packaging. A systematic investigation was made to  
73 determine the effect of r-CNCs on the optical, water vapor and O<sub>2</sub> barrier and tensile properties of  
74 gelatin films, and the results are compared with those using conventional (non-grafted) CNCs. To  
75 the best of our knowledge, the use in food packaging of mechanically-reinforced gelatin films with  
76 antimicrobial properties remains unexplored. We demonstrate the potential of gelatin films loaded  
77 with r-CNCs with agar diffusion tests and storage experiments using mozzarella cheese as a model  
78 food matrix.

79

## 80 2. MATERIALS AND METHODS

81

### 82 2.1. Materials

83       Bovine gelatin powder (Bloom Strength-180) was kindly supplied by Gelco Gelatinas do  
84 Brazil Ltda (Pedreira, SP). CNCs, isolated from wood pulp by sulfuric acid hydrolysis and  
85 delivered as a dried powder, were purchased from Celluforce Inc. (Windsor, Québec, Canada).  
86 Rosin was purchased from Aldrich Chemical (USA). Glycerol and ethanol were purchased from  
87 Across Organics (USA). All chemicals were of analytical grade and were used as purchased.  
88 *Staphylococcus aureus* (*S. aureus*, Gram-positive, ATCC 25923) and *Escherichia coli* (*E. coli*,  
89 Gram-negative, ATCC 25922) were supplied by Cefar Diagnostica (Brazil). Distilled water was  
90 used in all experiments.

91

### 92 2.2. Synthesis of rosin-grafted CNCs (r-CNCs)

93 The CNCs were functionalized with rosin by a SolReact (solvent-free) process adapted  
94 from Castro et al.[37]. In this process, carboxylic acids are the solvent and grafting agents at the  
95 same time. The water evaporation during the reaction provokes an in situ solvent exchange from  
96 water to the reactant, which allows for efficient esterification according to Le Chatelier's principle,  
97 and saturation of CNCs with the melted carboxylic acid at low pH [40]. The reaction mechanism is  
98 presented in Fig. S1 in the Supporting Information. 2.0 g of CNCs were dispersed in water at 1.0  
99 wt% and ultrasonicated for 2 min using a Branson sonicator, and the pH was adjusted to 4.0 with  
100 HCl (0.1 mol/L). The CNCs dispersion was placed in a closed distillation system in an oil bath at  
101 130 °C. After 10 min, 22.35 g of rosin (10 equiv. according to the CNCs dry weight) were added  
102 slowly to ensure its melting and adsorption on the CNCs surface. The system was kept under  
103 stirring for 9 h at 130 °C. After the reaction, the rosin-grafted CNCs (r-CNCs) were purified from  
104 unreacted rosin by six dispersion-centrifugation cycles (10000 rpm at 4 °C for 10 min) with a large  
105 excess of ethanol, until no more rosin was detected by FTIR in the supernatant. Afterward, the r-  
106 CNCs were recovered by centrifugation and washed thoroughly with water, and then sonicated for 5  
107 min and stored in a refrigerator. The final solid content was 3.5% (w/w).

108

### 109 **2.3. Preparation of gelatin/r-CNCs bionanocomposite films**

110 The bionanocomposite films were prepared by solvent casting. The gelatin powder was  
111 hydrated in distilled water (10 g/100 g) at 24 °C for 5 min and then heated at 60 °C under stirring  
112 for 15 min. Glycerol (20 wt% on a dry gelatin basis) was added to the gelatin solution under  
113 stirring. The solution obtained was mixed with the r-CNCs suspension at various contents (0 wt%,  
114 0.5 wt%, 4.0 wt% and 6.0 wt%, on a dry gelatin basis) and stirred for 5 min. The suspensions (45  
115 mL) were then cast on glass plates (40 × 25 cm) covered with a polyester film (Mylar®, DuPont,  
116 Brazil) to facilitate film peeling off after drying at room temperature for 24 h. Film samples were

117 conditioned at 50% RH and 25 °C for at least 24 h prior to testing. Gelatin films incorporated with  
118 non-grafted CNCs were prepared at the same concentrations described above for comparison.

119

## 120 **2.4. Characterization**

121

### 122 **2.4.1. Structural and morphological analyses of r-CNCs**

123 The functionalization of CNCs with rosin was characterized by X-ray photoelectron  
124 spectroscopy (XPS, XR3E2, Vacuum Generator, UK) equipped with monochromatic Mg K $\alpha$  X-ray  
125 source (1253.6 eV) operated at 15 kV and 20 mA. CNCs and r-CNCs were characterized by Fourier  
126 Transform Infrared Spectroscopy (FTIR, FT-NIR VERTEX spectrometer, Bruker, Germany) in the  
127 attenuated total reflection (ATR) mode. Spectra were recorded between 4000 and 400 cm<sup>-1</sup> with a  
128 resolution of 1 cm<sup>-1</sup> and 32 spectral accumulations. The FTIR measurements of gelatin films were  
129 carried out with five repetitions for each film sample. **PVC films were also characterized to  
130 compare the light transmission of the gelatin bionanocomposites with synthetic packaging films.**

131 The morphology of CNCs and r-CNCs was investigated using transmission electron microscopy  
132 (Tecnai<sup>TM</sup> G2 F20 microscope, FEI Company, USA) in the STEM (Scanning Transmission  
133 Electron Microscopy) mode with an accelerating voltage of 80 kV. The samples were prepared by  
134 depositing a 0.1 wt% suspension droplet on a carbon microgrid with formvar (400 mesh) stained  
135 with 1.5 wt% uranyl acetate solution. A minimum of 10 images was recorded and the most  
136 representative one was used for discussion. The CNCs and r-CNCs sizes were determined from the  
137 analysis of a minimum of 100 particles using the ImageJ software.

138 The crystallinity of CNCs and r-CNCs was estimated by X-ray diffraction (XRD,  
139 Panalytical diffractometer, X'Pert Pro MPD-Ray, The Netherlands) with Ni-filtered Cu K $\alpha$   
140 radiation ( $\lambda = 1.54 \text{ \AA}$ , 45 kV, 40 mA) in the  $2\theta$  range from 5° to 60°. The crystallinity index (CI)  
141 was calculated according to the Segal's equation [41]:

142  $CI (\%) = \left(1 - \frac{I_1}{I_2}\right) \times 100$  (1)

143

144 where  $I_1$  is the intensity at the minimum ( $2\theta = 18^\circ$ ) and  $I_2$  in the intensity associated with the  
145 crystalline region of cellulose ( $2\theta = 22.7^\circ$ ).

146

#### 147 **2.4.2. Morphological and optical analysis of CNCs and r-CNCs/gelatin films**

148 The film cross-sectional surface was studied using a JEOL Scanning Electron Microscope  
149 (SEM, model Quanta200, FEI, the Netherlands). The samples were first cryo-fractured in liquid  $N_2$   
150 and then fixed onto  $90^\circ$  specimen mounts to be coated with a ca. 5-nm-thick gold layer in an argon  
151 atmosphere. The SEM images were taken at accelerating voltages below 5 kV using the secondary  
152 electron mode. Polarization-modulation infrared reflection-absorption spectroscopy (PM-IRRAS)  
153 was conducted on a spectrophotometer (PMI 550, KSV Instruments, Finland). The light beam angle  
154 of incidence was  $81^\circ$ . An average of 600 scans was collected for each spectrum at resolution of 8  
155  $cm^{-1}$ . In the PM-IRRAS technique, the incoming light is continuously modulated between *s*- and *p*-  
156 polarization at a high frequency, so that the spectra for the two polarizations can be measured  
157 simultaneously. Therefore, the films were placed on an Au substrate and the PM-IRRAs spectra  
158 were obtained from the reflectivity components *s* and *p*, as given by Eq. 2:

159

160  $\Delta R/R = (R_p - R_s) / (R_p + R_s)$  (2)

161

162 where  $R_p$  is the reflectivity of the parallel component (*p*-polarization) and  $R_s$  is the reflectivity of  
163 the component perpendicular to the light plane of incidence (*s*-polarization). All measurements  
164 were carried out in a class 10,000 cleanroom at  $23 \pm 1^\circ C$ . Transmittance spectra were acquired in  
165 triplicate on a UV-1650 spectrophotometer (Model PC, Shimadzu, Kyoto, Japan) at wavelengths  
166 between 190 and 800 nm.

### 167 **2.4.3. Water vapor and O<sub>2</sub> barrier and tensile properties determinations**

168 The water vapor permeability (WVP) of the films was determined following ASTM E-96-  
169 01. The preconditioned film was sealed onto the opening of an aluminum permeation cup (28 mm  
170 internal diameter) containing dried calcium chloride. The cup was kept in a controlled chamber at  
171  $23 \pm 1$  °C and  $50 \pm 5\%$  RH. The cup was weighed at least four times for at least 7 days under this  
172 controlled environment. For each film, three replicates were performed. WVP [(g mm)/ m<sup>2</sup> h kPa]  
173 was determined using Eq. 3:

174

$$175 \text{ WVP} = \text{WVTR} \times L/\Delta p \quad (3)$$

176

177 in which WVTR is the water vapor transmission rate (g/m<sup>2</sup> h) through the film area; L is the film  
178 thickness (mm), and  $\Delta p$  is the partial pressure gradient (kPa) across the film.

179 The Oxygen Transmission Rate (OTR) of the films was determined in duplicate at 0%, 50%,  
180 and 80% RH according to the ASTM D3985 method (2002a) using an oxygen transmission rate  
181 analyzer (Systech Illinois 8500, USA). The tensile properties of the films were determined as per  
182 the ASTM D882-09 standard method (2009). Film specimens were prepared and equilibrated at  $23$   
183  $\pm 1$  °C and  $50 \pm 5\%$  RH for 48 h. The tests were carried out on an Instron Universal Testing  
184 Machine (model 5569, Instron Corp., USA) with a 100 N load cell. The specimens were stretched  
185 using crosshead speed of 10 mm/min with clamps initially separated by 100 mm. Tensile strength,  
186 Young's modulus, and elongation at break were calculated from the stress-strain curves. The tests  
187 were performed with five replicates for each film. Film thickness was measured with a digital  
188 micrometer (Mitutoyo Corp., Kanogawa, Japan) to the nearest 0.001 mm. At least 10 specimens of  
189 each composition were analyzed.

190

### 191 **2.4.4. Antimicrobial activity tests**

192 The bacterial strains to evaluate the effectiveness of CNCs- and r-CNCs-loaded gelatin  
193 solutions were *Staphylococcus aureus* and *Escherichia coli*, which are foodborne pathogens  
194 [42,43]. The inoculum cultures were prepared inoculating a selected single colony in 15 mL of  
195 Muller-Hinton Broth medium (MHB), followed by overnight incubation at 35 °C. The optical  
196 densities at 625 nm were measured by UV-Vis absorption spectroscopy and compared with the  
197 turbidity of a 0.5 McFarland standard at the same wavelength, equivalent to  $1.5 \times 10^8$  colony  
198 forming units per mL (CFU/mL). The overnight cultures were diluted in MHB until reaching  $10^6$   
199 CFU/mL. The antimicrobial activity of the CNCs and r-CNCs suspensions was assessed by  
200 determining the minimum inhibitory concentration (MIC) in a 96 flat-bottomed-well tissue culture  
201 microplate. Briefly, 100  $\mu$ L of sterile Mueller Hinton were added to all wells. In the first column,  
202 the wells were filled with 50  $\mu$ L of CNCs ( $50 \text{ mg}\cdot\text{ml}^{-1}$ ) and r-CNCs ( $22 \text{ mg}\cdot\text{ml}^{-1}$ ) suspensions. Then,  
203 50  $\mu$ L of each antimicrobial substance were serially transferred from the well to the corresponding  
204 wells. Then, 50  $\mu$ L of the culture suspension were added to all wells. Positive and negative controls  
205 (streptomycin and culture medium – data not shown) were included in each assay plate. Afterward,  
206 the inoculated plates were incubated in a wet chamber for 24 h at 35 °C and then chlorinated with  
207 50  $\mu$ L of 2,3,5-Triphenyltetrazolium chloride (0.1%). The lowest sample concentration with an  
208 inhibition effect on microbial growth was considered as the MIC for each tested microorganism. In  
209 the antimicrobial film test, all films were cut into discs of 10 mm diameter and both sides were  
210 sterilized by UV treatment in a laminar flow hood for 30 min. The discs were placed on Muller-  
211 Hinton Agar (MHA) plates that had been previously seeded with 100  $\mu$ L of inoculums containing *S.*  
212 *aureus* or *E. coli* at a concentration of  $1 \times 10^6$  CFU/mL. The plates were then incubated at 35 °C for  
213 24 h. Two independent experiments were performed in triplicate. The antibacterial activity of the  
214 gelatin/r-CNCs films on mozzarella cheese was also investigated. Fresh mozzarella samples (20  
215 mm x 20 mm x 10 mm; four replicates) were wrapped with gelatin and gelatin/r-CNCs films. All

216 samples were packaged, sealed and stored at room temperature for 1 month. Cheese samples  
217 without film and wrapped in PVC cling film were used as control.

218

#### 219 **2.4.5. Statistical analysis**

220

221 All data were subjected to analysis of variance (ANOVA). Mean values were compared  
222 using the Tukey's test at a confidence level of 95% ( $p < 0.05$ ).

223

### 224 **3. RESULTS AND DISCUSSION**

225

#### 226 **3.1. Functionalization of CNCs with rosin**

227

228 The surface functionalization of CNCs with rosin was confirmed by XPS (Fig. 1a-b) and  
229 FTIR (Fig. 1c). The full XPS spectra of CNCs and r-CNCs show that the surfaces of both samples  
230 contained mainly carbon and oxygen atoms (signals at 248 and 532 eV, respectively). The C1s  
231 signal was deconvoluted to quantify the relative abundance of the carbon atom types, which  
232 displayed 4 peaks attributed to C1 (C-C at 285.0 eV), C2 (C-O at 286.6 eV), C3 (O-C-O at 288.0  
233 eV) and C4 (-O-C=O at 289.1 eV) [44]. The esterification of CNCs surface with rosin changed the  
234 relative proportion of C4 and C1 peaks due to the higher amount of aliphatic carbon from rosin.  
235 Furthermore, the O/C ratio decreased from 0.61 to 0.33 (Table 1), also confirming the successful  
236 grafting of rosin onto the CNCs. Niu et al. [39] found similar behavior for rosin-modified cellulose  
237 nanofibers. The chemical grafting of CNCs with rosin was analyzed by ATR-FTIR (Fig. 1c).  
238 Typical vibration bands of cellulose were observed in the CNCs and r-CNCs spectra, including O-H  
239 stretching at  $3340\text{ cm}^{-1}$ , C-H symmetrical stretching at  $2895\text{ cm}^{-1}$ , H-O-H bending of absorbed  
240 water molecules at  $1647\text{ cm}^{-1}$ ,  $\text{CH}_2$  symmetrical bending at  $1427\text{ cm}^{-1}$ , and C-O-C vibration on

241 glycosidic linkages at  $1165\text{ cm}^{-1}$  [37,39]. After chemical grafting, a new band at  $1740\text{ cm}^{-1}$  was  
 242 observed in the spectrum of r-CNCs, assigned to ester carbonyl groups from the reaction between  
 243 the OH groups of CNCs and  $-\text{COOH}$  groups of rosin. Likewise, the increased intensity of the band  
 244 at  $1647\text{ cm}^{-1}$  can be related to  $\text{C}=\text{C}$  stretching from rosin cyclic alkene rings, which was also  
 245 observed by PM-IRRAS. There was no significant reduction in the intensity of the OH band at  $3340$   
 246  $\text{cm}^{-1}$ , indicating that esterification occurred mainly with hydroxyl groups accessible at the CNCs  
 247 surface, as reported by Castro et al. [37]. The absence of a band at  $\sim 1700\text{ cm}^{-1}$  from rosin carbonyl  
 248 groups indicates that the residual rosin was completely removed after the purification step. The  
 249 TEM images of CNCs and r-CNCs in Fig. 1d-e show that the needle-like shape of the nanocrystals  
 250 was unchanged after functionalization with rosin, as expected. The average lengths for CNCs and r-  
 251 CNCs were  $108.0 \pm 33$  and  $122.0 \pm 50$  nm, and the average diameters were  $3.8 \pm 0.9$  and  $7.5 \pm 2.2$   
 252 nm, respectively. The largest dimensions of r-CNCs are attributed to the small aggregates of CNCs  
 253 crystals. This is consistent with Espino-Pérez et al. [28] who observed the largest length for  
 254 octadecyl isocyanate-grafted CNCs (179.0 nm) compared with non-grafted CNCs (155.0 nm). A  
 255 schematic representation of the rosin-functionalized CNCs is shown in Fig. 1f.

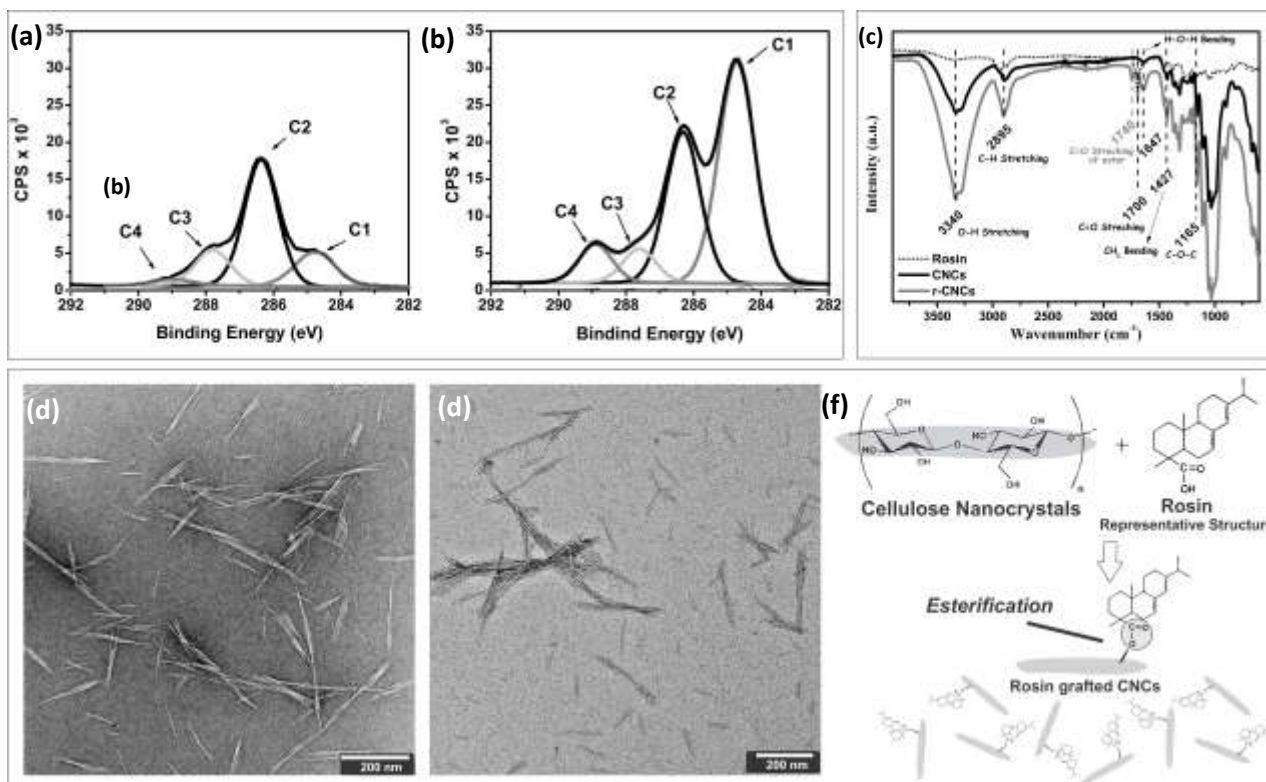
256

257 Table 1: X-ray photoelectron spectroscopy data of CNCs and r- CNCs

Cellulose nanoparticles	O/C	Binding energy, eV			
		C1: C-C 285.0	C2: C-O 286.6	C3: O-C-O 288.0	C4: O=C-O 289.1
CNCs	0.61	16.4	62.6	17.2	3.8
r-CNCs	0.33	52.1	32.5	7.3	8.1

258

259



260  
 261 Fig. 1. C<sub>1s</sub> XPS spectra of (a) CNCs and (b) r-CNCs. (c) ATR-FTIR spectra of rosin, CNCs, and r-  
 262 CNCs. (d) TEM micrographs of CNCs and (e) r-CNCs. (f) schematic representation of rosin-  
 263 functionalized CNCs.

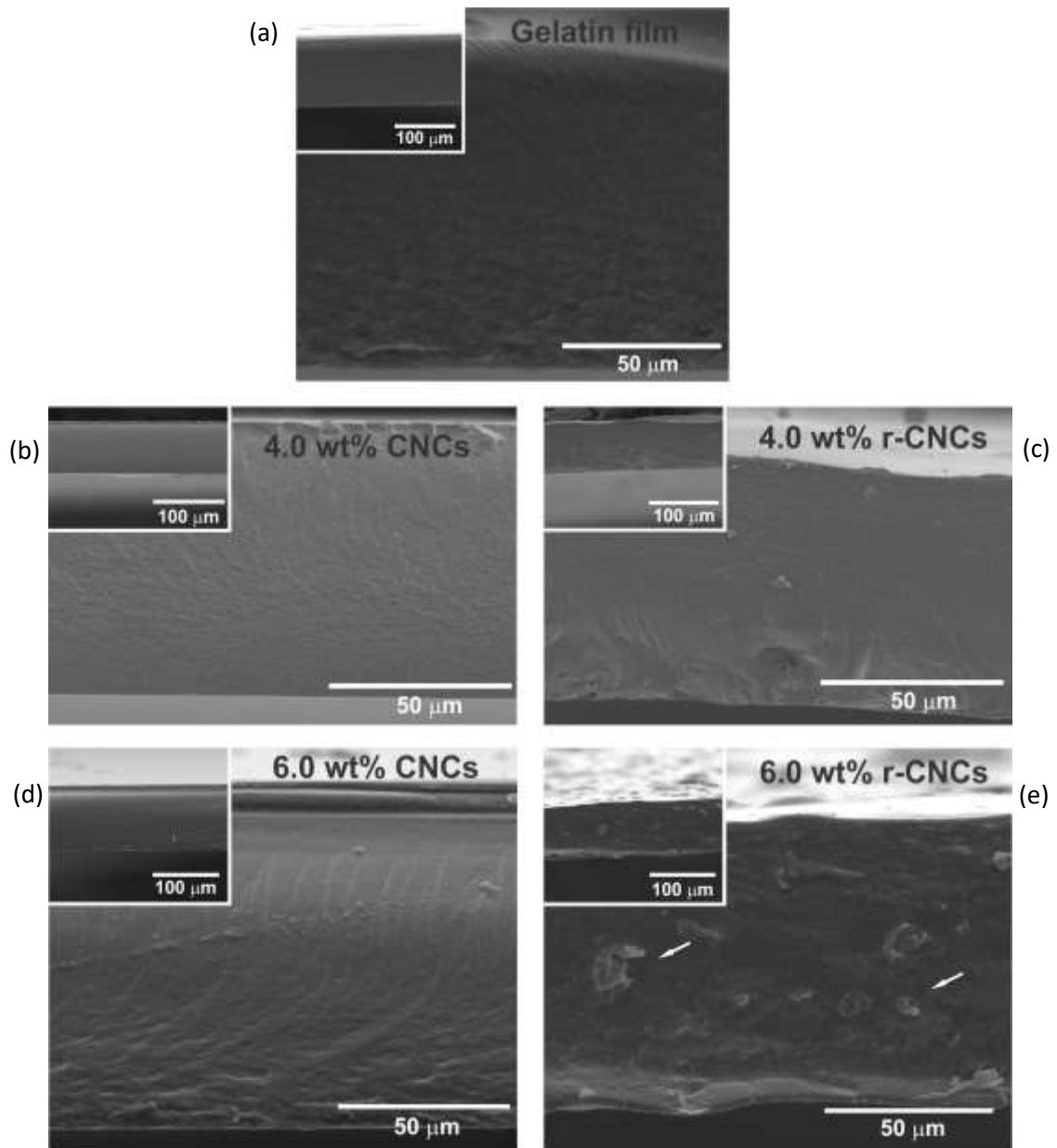
264  
 265 The XRD patterns of CNCs and r-CNCs are displayed in Fig. S2 in the Supporting  
 266 Information. Both samples exhibited typical diffraction peaks at  $2\theta = 16.5, 22.7, \text{ and } 34.8^\circ$ , related  
 267 to cellulose I polymorph [37]. This confirms that rosin grafting did not convert cellulose I into  
 268 cellulose II. The crystallinity index slightly increased from 82% to 84% after functionalization.  
 269 Similar behavior was reported by Niu et al. [39], who found crystallinity indexes of 59.91 and  
 270 63.42% for CNF and rosin-CNF, respectively. These increases in crystallinity were attributed to the  
 271 partial hydrolysis of the nanocellulose amorphous phase due to the acidic condition used in the  
 272 reaction with rosin [39].

273

### 274 3.2. Morphology and optical properties of gelatin films reinforced with CNCs and r-CNCs

275 Pure gelatin and bionanocomposite films of different CNCs and r-CNCs contents were  
276 obtained with solution casting. The thickness of the free-standing films was similar ( $\sim 85 \mu\text{m}$ ) for  
277 all compositions with standard deviations lower than 20%. The dispersion of CNCs and r-CNCs in  
278 the gelatin matrix was studied by SEM, as shown in Fig. 2. The gelatin films with low CNCs  
279 content had smooth and more regular surfaces. The absence of agglomerates for the film with 4.0  
280 wt% r-CNCs content is suggested from the SEM image in Fig. 2c, indicating a good dispersion of r-  
281 CNCs [45] within the gelatin matrix. Nevertheless, agglomerates appeared when 6.0 wt% r-CNCs  
282 were added to the gelatin film (Fig. 2e). This is probably due to the increased hydrophobicity of r-  
283 CNCs after functionalization with rosin, which decreased chemical compatibility with the  
284 hydrophilic gelatin matrix. The evidence of increased hydrophobicity in gelatin/r-CNCs films is  
285 provided by contact angle measurements (Fig. S3 in the Supporting Information).

286



287  
 288 Fig. 2. SEM micrographs of the cross-sectional surface of (a) pure gelatin film and gelatin  
 289 bionanocomposites with 4.0 wt% (b) CNCs and (c) r-CNCs, and with 6.0 wt% (d) CNCs and (e)  
 290 CNCs content.

291  
 292 Polarization-modulated infrared reflection-absorption spectroscopy (PM-IRRAS) was  
 293 performed to infer filler/matrix interactions in the CNCs- and r-CNCs-based gelatin  
 294 bionanocomposites [46]. The PM-IRRAS signal has an overall dependence on the number of  
 295 chemical group dipoles at the sample surface and on the orientation of these dipoles. Fig. 3 shows

296 representative PM-IRRAS spectra for the pure gelatin film and bionanocomposite films containing  
297 6.0 wt% CNCs or r-CNCs. The bands and calculated areas are summarized in Table S1 and Fig. S4,  
298 respectively, in the Supporting Information. For the pure gelatin film, the spectrum displays typical  
299 bands of gelatin structure. The bands at 1388, 1523 and 1755/1760  $\text{cm}^{-1}$  are ascribed to amide III,  
300 amide II (60% N-H and 40% C-N) and C=O dipoles, respectively [47–49], while the band at 1625  
301  $\text{cm}^{-1}$  may be attributed to amide I (80% C=O, 10% N-H and 10% C-N). These bands also appeared  
302 in the PM-IRRAS spectra of the bionanocomposites, but their areas were slightly reduced with the  
303 addition of 6 wt% CNCs, most likely because of the total gelatin content in the film decreased from  
304 83 to 79%. An opposite trend was observed for the 6 wt% r-CNCs-loaded gelatin  
305 bionanocomposite, whose spectrum showed that the area/intensity of the amide bands increased,  
306 suggesting dipole reorientation in the presence of r-CNCs. There was also a contribution of the C=C  
307 dipoles from the rosin alkene rings on the amide I band intensity [47–49]. The spectral range  
308 ascribed to C=O dipoles was also modified in the spectrum, with larger area reduction for the band  
309 at 1755/1760  $\text{cm}^{-1}$  than in the other samples. In addition, there was a new band at 1712  $\text{cm}^{-1}$ , which  
310 can be assigned to the ester carbonyl (C=O) groups from the r-CNCs, as already observed by ATR-  
311 FTIR. The PM-IRRAS spectra reveal that the chemical environment of the dipole-forming gelatin  
312 groups was more effectively disturbed with r-CNCs rather than with CNCs. This suggests that the  
313 filler/matrix interactions in the gelatin/r-CNCs bionanocomposites encompass dipole-dipole  
314 interactions in addition to hydrogen bonding, which is the only chemical interaction expected in the  
315 case of CNCs.

316

317

318

319

320

321  
322  
323  
324  
325  
326  
327  
328  
329  
330  
331  
332  
333  
334  
335  
336  
337  
338  
339  
340

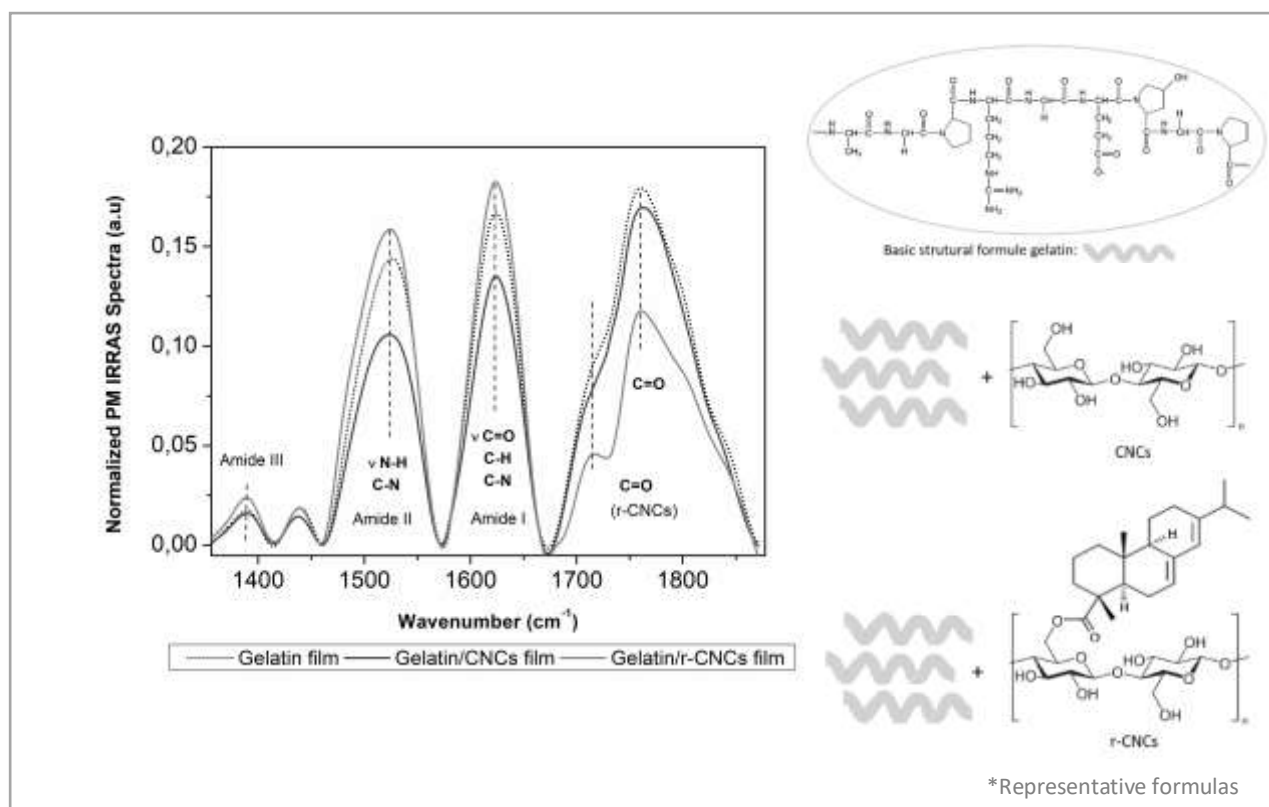
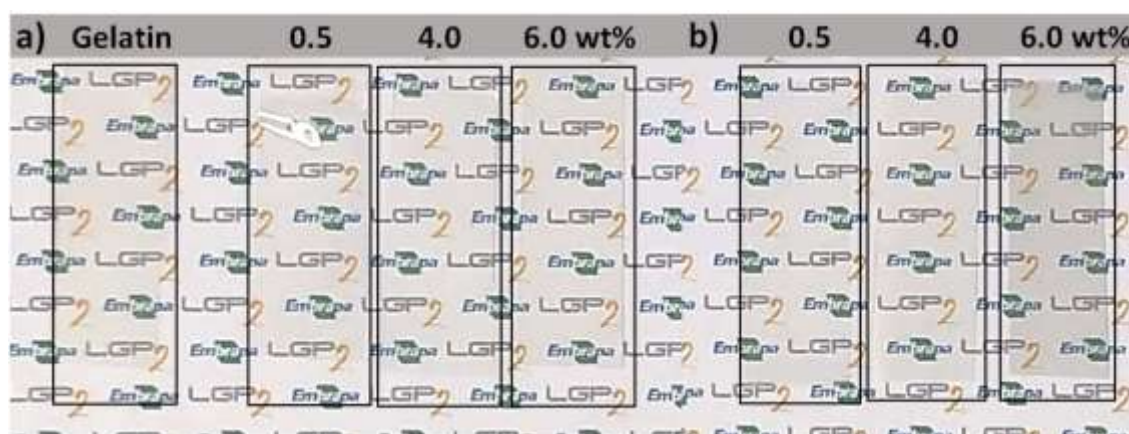


Fig. 3: PM-IRRAS spectra of gelatin film and gelatin bionanocomposites with 6 wt% CNCs and 6 wt% r-CNCs. The spectrum of a clean gold substrate was used as a baseline.

All gelatin/CNCs and gelatin/r-CNCs bionanocomposites were flexible, and exhibited good macroscopic homogeneity and high light transparency, as displayed in Fig. 4 and in the UV-Vis transmittance spectra in Fig. S5 in the Supporting Information. The gelatin film exhibited a high barrier against UV radiation, nearly 100% for UVC, over 93.3% for UVB, and 54.0% for UVA, due to chromophore groups such as tyrosine and phenylalanine [50]. The addition of r-CNCs led to a significant reduction in the transmittance over all the UV range compared to the neat gelatin and gelatin/CNCs film samples. The gelatin film with 0.5 wt% r-CNCs showed a reduction of 20.8 and 29.1 % in the UVB and UVA transmittance, respectively, compared to the gelatin/CNCs films. Narayanan et al. [36] observed a reduction of 1% and 6% for UVB and UVA, respectively, in PLA bionanocomposites with 20 wt% rosin. The authors attributed this behavior to the absorption properties of rosin, which prevented light transmission through the films. However, the gelatin film

341 with 6.0 wt% r-CNCs showed a significant reduction in the visible light range, which indicates light  
 342 scattering by r-CNCs aggregates, as shown in the SEM images (Fig. 2e). Table 2 presents a  
 343 comparison of light transmission between the gelatin/r-CNCs bionanocomposites and some  
 344 synthetic packaging films. The gelatin/r-CNCs films had low transmittance over the entire spectral  
 345 range, indicating that they absorbed light much more efficiently than several synthetic polymer  
 346 films. These results suggest that the gelatin/r-CNCs bionanocomposites are suitable as packaging to  
 347 protect light-sensitive food products.

348



349

350 Fig. 4. Photography of (a) gelatin/CNCs and (b) gelatin/r-CNCs bionanocomposite films

351

352 Table 2: Optical properties of gelatin/r-CNCs bionanocomposites and synthetic packaging films.

Film	Light transmission (%)			
	200 nm	280 nm	400 nm	600 nm
0.5 wt% gelatin/r-CNCs	0.0	4.5	77.3	87.4
6.0 wt% gelatin/r-CNCs	0.0	5.4	60.5	66.7
Synthetic films currently applied in food packaging <sup>a</sup>				
LDPE <sup>a</sup>	13.1	67.5	83.4	86.9
OPP <sup>a</sup>	4.6	80.0	87.9	89.1
PVC	20	83.9	87.9	88.7

353 LDPE: low-density polyethylene; OPP: oriented polypropylene; PVC: poly(vinyl chloride)

354 <sup>a</sup> adapted from [51].

355

### 3.3. Barrier and mechanical properties of gelatin/CNCs and gelatin/r-CNCs films

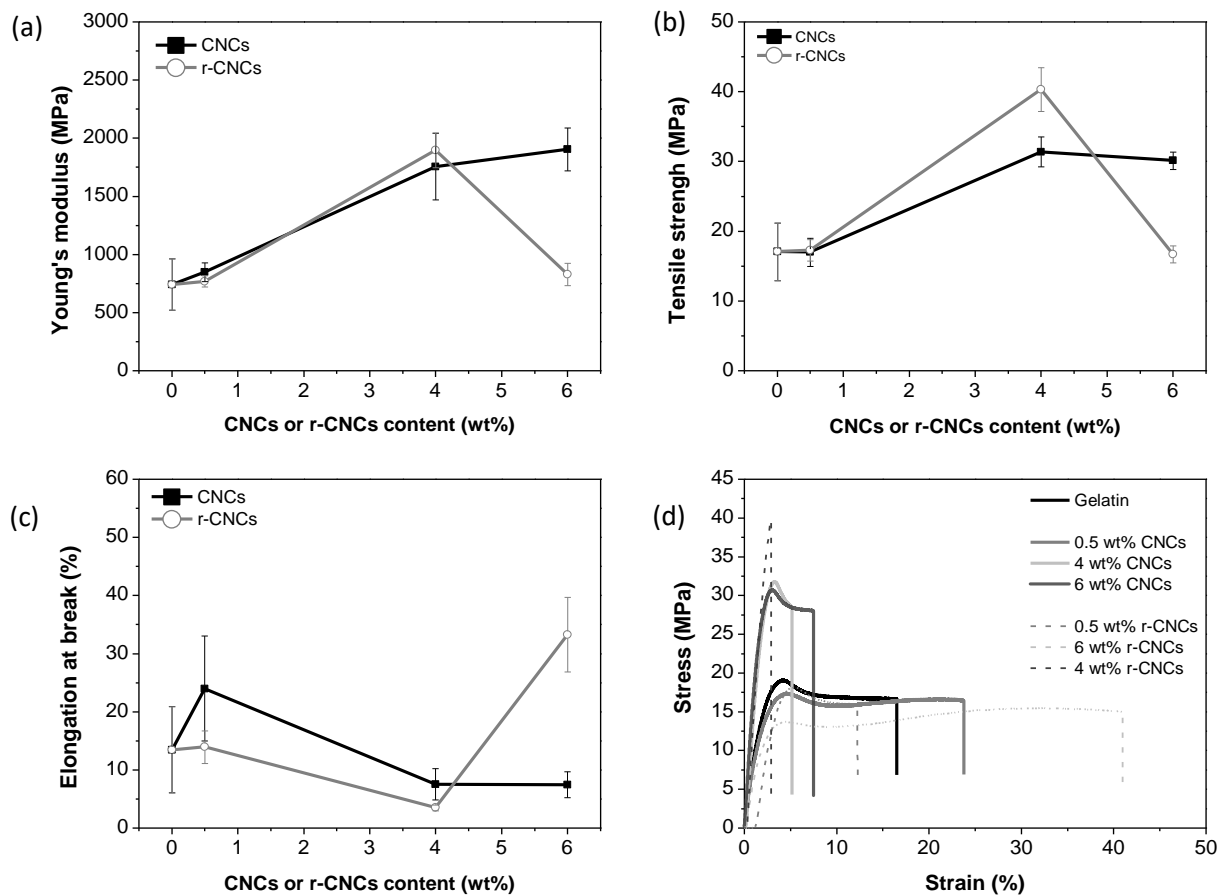
Water vapor permeability (WVP) and oxygen transmission rate (OTR) are barrier properties that determine the ability of bio-based films to protect food products from moisture and O<sub>2</sub> transfer, lipid oxidation, and loss of volatile aromas and flavors. Gelatin films generally display good barrier against oxygen at low and intermediate relative humidity [52]. Our results show that the OTR of the gelatin films with 0.5 and 6.0 wt% CNCs and r-CNCs at 0% and 80% RH were < 0.01 cm<sup>3</sup>/m<sup>2</sup>.day, indicating that the addition of CNCs or r-CNCs did not change significantly the already high oxygen barrier of gelatin. The values of WVP and WVTR of the gelatin bionanocomposites with CNCs and r-CNCs at 25 °C and 50% RH are presented in Fig. S6 in the Supporting Information. The pure gelatin film exhibited a WVP of 0.20 ± 0.03 g mm/m<sup>2</sup> h kPa. The incorporation of CNCs or r-CNCs reduced the WVP of the gelatin films. The addition of 0.5 wt% r-CNCs significantly decreased the WVP by 55% (p < 0.05). According to Ooi, Ahmad, & Amin [53], nanoparticles can reduce WVP by increasing the biopolymer crystallinity or by reducing the free hydrophilic groups (OH, NH) in the gelatin matrix, thereby creating a tortuous pass for water vapor diffusion through the film matrix. Santos et al. [54] reported decreased WVP of protein films with increasing CNCs content. They found that fish gelatin films with 15 wt% CNCs had WVP values of approximately 2 g mm/m<sup>2</sup> h kPa (25 °C at 85% RH). George & Siddaramaiah [24] reported that 4.0 wt% bacterial cellulose nanocrystals reduced WVP of gelatin, and attributed this outcome to the low hygroscopicity of highly crystalline CNCs. They found WVP values of around 0.175 g mm/m<sup>2</sup> h kPa (25 °C at 50% RH), which were higher than those of our gelatin films reinforced with CNCs or r-CNCs.

The mechanical properties (Young's modulus, tensile strength, and elongation at break) of the bionanocomposite films were investigated with tensile tests. The Young's modulus and tensile strength of the pure gelatin film were 743 and 17 MPa, respectively, as shown in Fig. 5. For gelatin/CNCs bionanocomposite films, the tensile strength and Young's modulus increased

381 significantly with increasing the CNCs content. This can be attributed to the effective CNCs  
382 reinforcing effect through stress transfer from the gelatin matrix to CNCs [21]. For the same filler  
383 content of 4.0 wt%, the gelatin film with r-CNCs exhibited tensile strength ~30% higher than that of  
384 the film with CNCs. This improvement is likely due to van der Waals forces (e.g. dipole-dipole  
385 interactions) and hydrogen bonds between the r-CNCs and gelatin matrix. However, for gelatin/r-  
386 CNCs film with 6.0 wt% r-CNCs, a reduction in Young's modulus and tensile strength was  
387 observed. In addition, there was an increase in elongation at break, which can be attributed to the  
388 formation of agglomerates, as revealed by SEM. The gelatin film with 6.0 wt% r-CNCs showed an  
389 elongation at break ~145% higher than that of the pure gelatin film, indicating that the gelatin/r-  
390 CNCs films were much more ductile and flexible. The interaction formed between the gelatin and r-  
391 CNCs weakened the protein-protein interactions, which were effective in stabilizing the gelatin  
392 network, as described by Zhuang et al [22]. Therefore, it is clear that r-CNCs play an effective role  
393 in enhancing the mechanical properties of gelatin, with promising features for flexible food  
394 packaging.

395

396



397  
 398 Fig. 5. (a) Young's modulus, (b) tensile strength (c) elongation at break, and (d) stress-strain  
 399 curves as a function of CNCs and r-CNCs content in bionanocomposite gelatin films obtained by  
 400 casting.

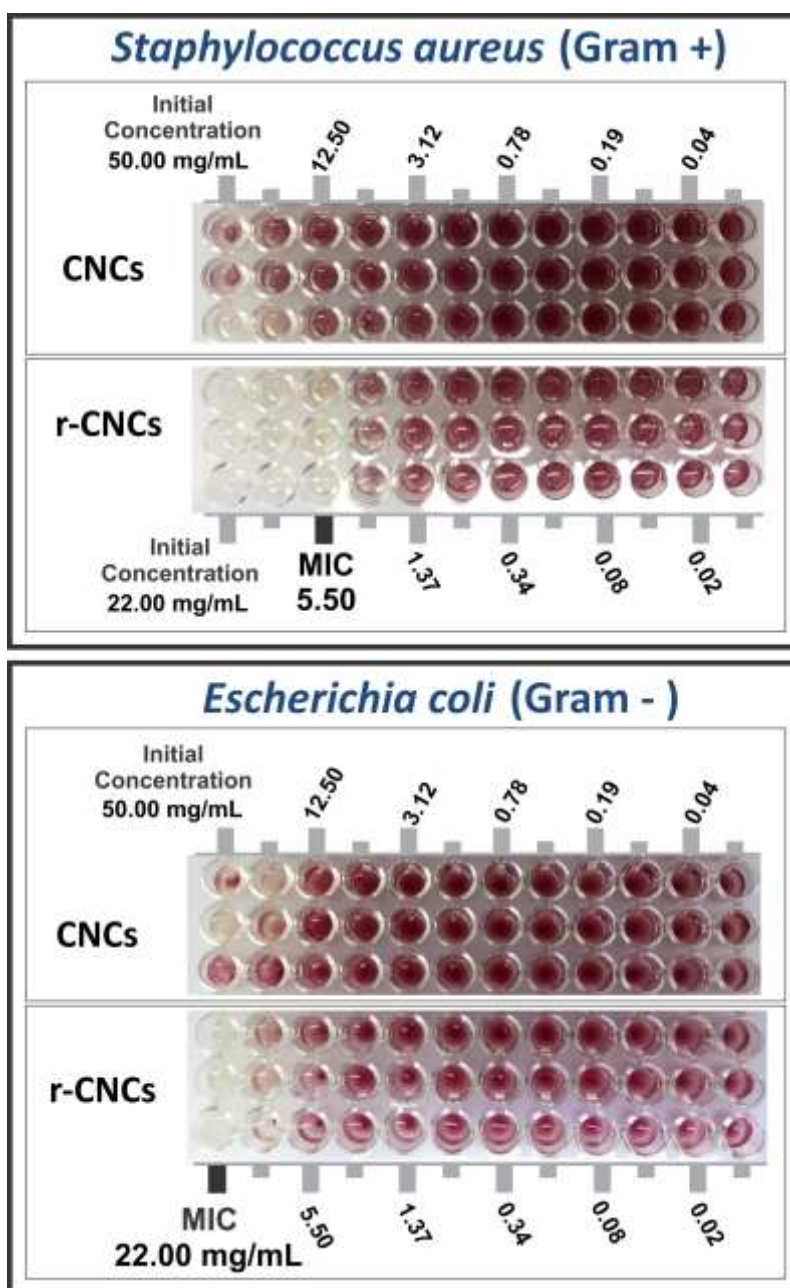
401

### 402 3.4. Antimicrobial properties of r-CNCs and gelatin/r-CNCs films

403

404 The minimum inhibitory concentration (MIC) value was determined as the lowest  
 405 concentration of r-CNCs suspension that inhibited the growth of the tested microorganisms. The  
 406 results in Fig. 6 show the highest bactericidal effect against Gram-positive *Staphylococcus aureus*  
 407 and Gram-negative *Escherichia coli* with the r-CNCs suspension. As expected, there was no  
 408 inhibitory effect for the CNCs suspension. A low concentration of r-CNCs (5.5 mg/mL) inhibited  
 409 the growth of *S. aureus*, whereas for *E. coli* inhibition a concentration of 22 mg/mL was required.  
 410 This may be due to the external lipopolysaccharide layer of the cell membrane of Gram-negative

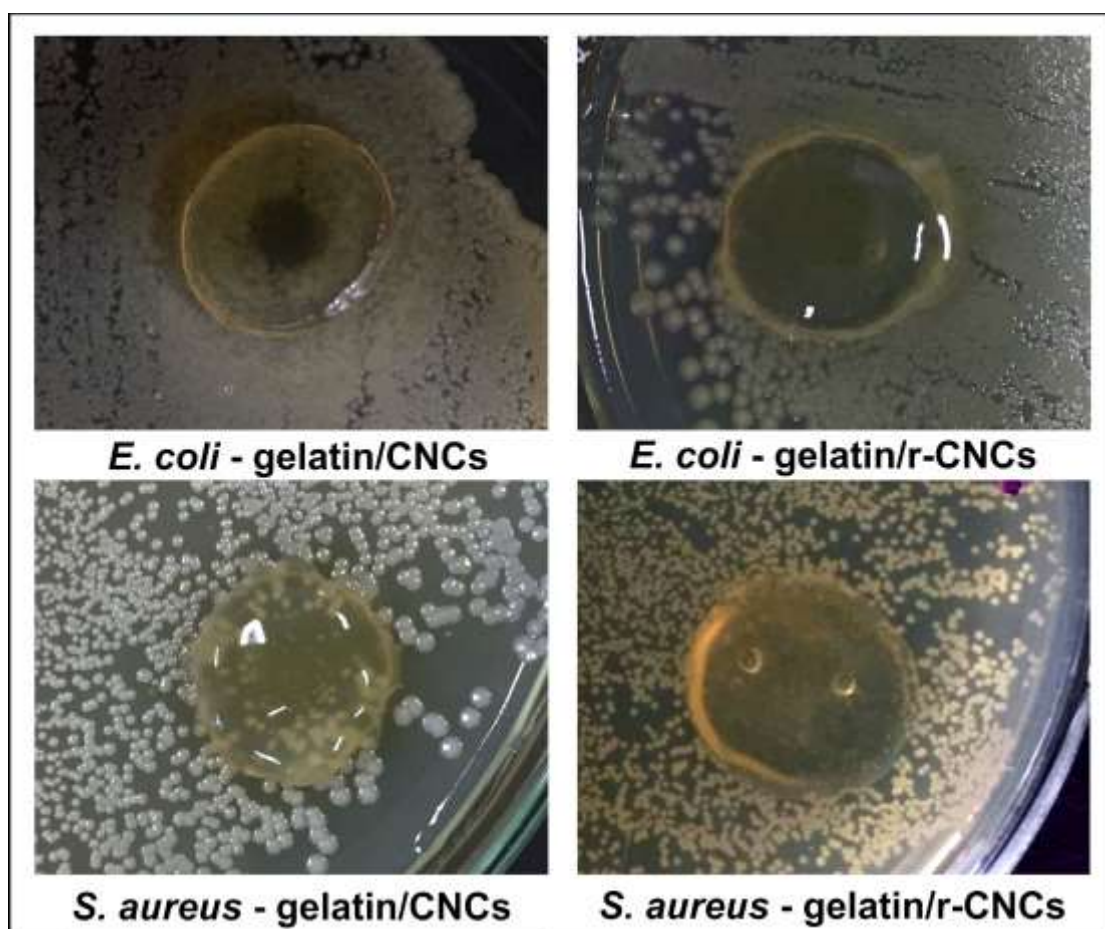
411 bacteria, which restricts diffusion of hydrophobic compounds [55]. The proposed mechanism for  
412 the r-CNCs antimicrobial activity is based on its interaction with the phospholipid cell membrane,  
413 which causes increased permeability and leakage of cytoplasm, or its reaction with enzymes located  
414 at the cell wall [56]. This is consistent with findings that rosin-derived cationic compounds have  
415 antimicrobial activity against many bacteria due to the hydrophobicity and structure of resin acids  
416 [57].



417

418 Fig. 6. Minimum inhibitory concentration (MIC) of CNCs and r-CNCs suspension tested on  
419 Gram-positive *Staphylococcus aureus* and Gram-negative *Escherichia coli*.

420 The gelatin/r-CNCs films were also tested against *S. aureus* and *E. coli* as demonstrated by  
421 the agar diffusion assays depicted in Fig. 7. The control films made with CNCs in gelatin did not  
422 display any inhibitory effect, with bacteria observed underneath. On the other hand, the gelatin/r-  
423 CNCs films showed an effective antibacterial property, especially against *E. coli*, since there was no  
424 bacterial growth in the inhibition area covered with the films. Neither of the tested films yielded a  
425 halo or a surrounding clearing zone, which shows that r-CNCs do not diffuse through the adjacent  
426 agar media and their antimicrobial effect is likely to occur by contact. The lack of diffusion is  
427 related to the hydrophobic nature of rosin molecules grafted onto the r-CNCs. Indeed, migration is  
428 linked to factors such as molecule size, polarity, shape, and quantity of water in the agar, in addition  
429 to the chemical structure and crosslinking in the films [58].

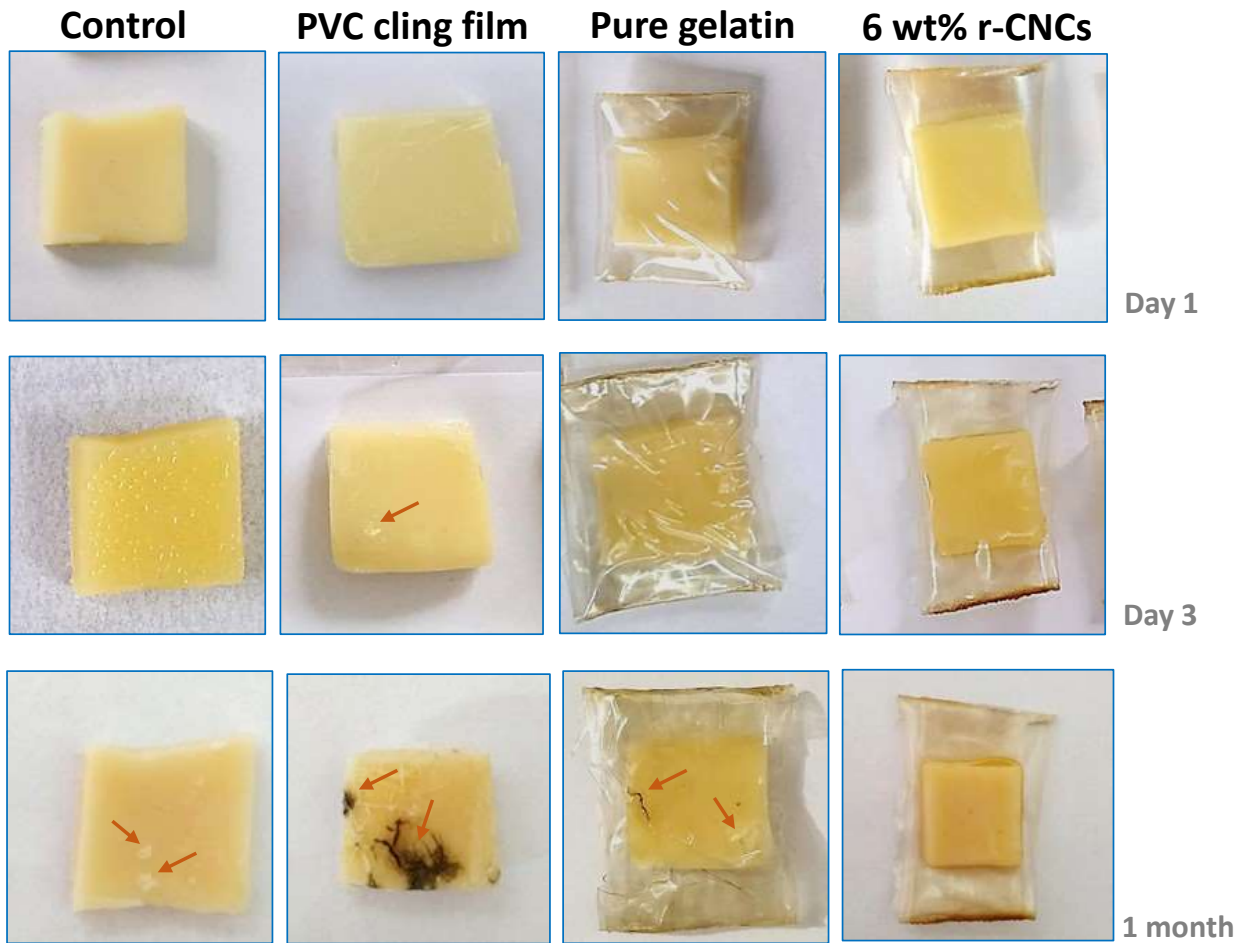


430

431 Fig. 7. Agar overlay assay of gelatin film discs against *S. aureus* and *E. coli*.

### 432 **3.5. Use of gelatin films reinforced with r-CNCs as packaging materials**

433  
434 Accelerated storage tests were carried out at 25 °C for one month to prove the antimicrobial  
435 ability of gelatin/r-CNCs films in practical applications. The tests were conducted with mozzarella  
436 cheese samples packed with pure gelatin, 6 wt% r-CNCs gelatin film, and a PVC film. Mozzarella  
437 cheese is perishable and suffers either from fungal or bacterial spoilage depending on the storage  
438 conditions. Fig. 8 shows evident microbial spoilage in the control and gelatin-packed cheese  
439 samples, and especially in the sample packed in PVC. In contrast, there was no microbial growth in  
440 the sample packed in 6 wt% r-CNCs-loaded gelatin film. As a proof of concept, we illustrated that  
441 the gelatin/r-CNCs bionanocomposite films can extend the shelf-life of mozzarella cheese, also  
442 providing a direct indication of the antibacterial activity of r-CNCs even after forming  
443 nanocomposites with gelatin. However, it is possible that r-CNCs migrated towards the oily cheese  
444 surface in contact with the film, but this has to be confirmed with further quantitative studies.



445  
 446 Fig. 8: Schematic comparison of accelerated storage for mozzarella cheese slices packed in a  
 447 PVC cling film, pure gelatin film, and gelatin/r-CNCs nanocomposite (6 wt%) film over 30 days at  
 448 25 °C. The control refers to free-standing, unpacked cheese slices (The Brazilian version of  
 449 mozzarella cheese can be sliced, in contrast to the Italian mozzarella). Microbial spoilage is  
 450 indicated by arrows in the images.

451  
 452 4. CONCLUSION

453  
 454 CNCs were successfully functionalized with rosin and used as a bactericidal nanofiller in  
 455 gelatin for achieving multifunctional packaging. In particular, the r-CNCs consistently improved the  
 456 optical, and water vapor barrier properties of gelatin films as compared to conventional CNCs. The  
 457 mechanical strength of the gelatin matrix was increased and could be tuned by varying the r-CNCs

458 content. This study demonstrates how grafting reactions can extend the functionalities of  
459 nanocelluloses for use in flexible packaging materials, which otherwise would suffer from limited  
460 physical and biological properties. **The results from microbial assays confirmed the potential of**  
461 **gelatin/r-CNCs nanocomposites in increasing the shelf-life of cheese samples. We expect that these**  
462 **findings will serve as a basis for future design of new functionalized nanocellulose/gelatin films for**  
463 **food storage under various conditions.**

464

465 ASSOCIATED CONTENT

#### 466 **Supporting Information**

467 Chemical mechanism for functionalization of cellulose nanocrystals with carboxylic acids (Fig. S1);  
468 XRD results (Fig.S2); contact-angle results (Fig.S3); Calculated area from the PM-IRRAS spectra  
469 (Fig.S4), PM-IRRAS band positions (Table.S1), UV-Vis spectra (Fig.S5), WVP and WVTR results  
470 (Fig.S6) (PDF).

471

472 AUTHOR INFORMATION

#### 473 **Corresponding Author**

474 \*E-mail: Julien.Bras@rd.nestle.com. Address: Nestle Research Center, 57 route du Jorat 1010,  
475 Lausanne, Switzerland. Phone: +33 7 86 05 24 45.

#### 476 **ORCID**

477 Julien Bras: 0000-0002-2023-5435

#### 478 **Author Contributions**

479 The manuscript was written through contributions of all authors. All authors have given approval to  
480 the final version of the manuscript.

#### 481 **Notes**

482 The authors declare no competing financial interest.

483

## 484 ACKNOWLEDGEMENTS

485 This research was made possible thanks to the facilities of the Laboratory of Pulp and Paper  
486 Science and Graphic Arts (LGP2) that is part of the LabEx Tec 21 (Investissements d’Avenir - grant  
487 agreement n°ANR-11-LABX-0030) and of PolyNat Carnot Institute (Investissements d’Avenir -  
488 grant agreement n° ANR-16-CARN-0025- 0), and Plant Macromolecule Research Center  
489 (CERMAV) for the support to this work. This study was financed in part by CNPq, SISNANO  
490 (MCTI), FINEP, Embrapa AgroNano research network (Embrapa), Coordenação de  
491 Aperfeiçoamento de Pessoal de Nível Superior - Brazil (CAPES) [Finance Code 001] and by the  
492 São Paulo Research Foundation (FAPESP) [grant numbers 2016/03080-2, 2017/18725-2 and  
493 2018/00278-2, 2018/10899-4, 2018/22214-6, 2018/18953-8]. We would like to thank Berthine  
494 Khelifi , Cécile Sillard and Thierry Encinas from Grenoble Institute of Technology for their  
495 expertise in providing SEM imaging, XPS and XRD analyses, respectively.

496

## 497 ABBREVIATIONS

498 CNCs Cellulose nanocrystals, r-CNCs cellulose nanocrystals functionalized with rosin

## 499 REFERENCES

500

- 501 [1] N.A. Al-Tayyar, A.M. Youssef, R. Al-hindi, Antimicrobial food packaging based on  
502 sustainable Bio-based materials for reducing foodborne Pathogens: A review, Food Chem.  
503 310 (2020) 125915. <https://doi.org/10.1016/j.foodchem.2019.125915>.
- 504 [2] S. Shankar, X. Teng, G. Li, J. Rhim, Preparation, characterization, and antimicrobial activity  
505 of gelatin/ZnO nanocomposite films, Food Hydrocoll. 45 (2015) 264–271.  
506 <https://doi.org/10.1016/j.foodhyd.2014.12.001>.
- 507 [3] F. Garavand, M. Rouhi, S.H. Razavi, I. Cacciotti, R. Mohammadi, Improving the integrity of  
508 natural biopolymer films used in food packaging by crosslinking approach: A review, Int. J.

- 509 Biol. Macromol. 104 (2017) 687–707. <https://doi.org/10.1016/j.ijbiomac.2017.06.093>.
- 510 [4] B. Hassan, S.A.S. Chatha, A.I. Hussain, K.M. Zia, N. Akhtar, Recent advances on  
511 polysaccharides, lipids and protein based edible films and coatings: A review, *Int. J. Biol.*  
512 *Macromol.* 109 (2018) 1095–1107. <https://doi.org/10.1016/j.ijbiomac.2017.11.097>.
- 513 [5] S. Sivakanthan, S. Rajendran, A. Gamage, T. Madhujith, S. Mani, Antioxidant and  
514 antimicrobial applications of biopolymers: A review, *Food Res. Int.* 136 (2020).  
515 <https://doi.org/10.1016/j.foodres.2020.109327>.
- 516 [6] J. Gómez-Estaca, C. López-de-Dicastillo, P. Hernández-Muñoz, R. Catalá, R. Gavara,  
517 Advances in antioxidant active food packaging, *Trends Food Sci. Technol.* 35 (2014) 42–51.  
518 <https://doi.org/10.1016/j.tifs.2013.10.008>.
- 519 [7] J.W. Han, L. Ruiz-Garcia, J.P. Qian, X.T. Yang, Food Packaging: A Comprehensive Review  
520 and Future Trends, *Compr. Rev. Food Sci. Food Saf.* 17 (2018) 860–877.  
521 <https://doi.org/10.1111/1541-4337.12343>.
- 522 [8] J. Wang, J. Fang, L. Wei, Y. Zhang, H. Deng, Y. Guo, C. Hu, Y. Meng, Decrease of  
523 microbial community diversity, biogenic amines formation, and lipid oxidation by phloretin  
524 in Atlantic salmon fillets, *Lwt.* 101 (2019) 419–426.  
525 <https://doi.org/10.1016/j.lwt.2018.11.039>.
- 526 [9] H. Moustafa, A.M. Youssef, N.A. Darwish, A.I. Abou-Kandil, Eco-friendly polymer  
527 composites for green packaging: Future vision and challenges, *Compos. Part B Eng.* 172  
528 (2019) 16–25. <https://doi.org/10.1016/j.compositesb.2019.05.048>.
- 529 [10] S. Esteghlal, M. Niakousari, S.M.H. Hosseini, Physical and mechanical properties of gelatin-  
530 CMC composite films under the influence of electrostatic interactions, *Int. J. Biol.*  
531 *Macromol.* 114 (2018) 1–9. <https://doi.org/10.1016/j.ijbiomac.2018.03.079>.
- 532 [11] X. Liu, Z. Ji, W. Peng, M. Chen, L. Yu, F. Zhu, Chemical mapping analysis of compatibility  
533 in gelatin and hydroxypropyl methylcellulose blend films, *Food Hydrocoll.* 104 (2020)

- 534 105734. <https://doi.org/10.1016/j.foodhyd.2020.105734>.
- 535 [12] Z. Wang, J. Zhou, X. xuan Wang, N. Zhang, X. xiu Sun, Z. su Ma, The effects of  
536 ultrasonic/microwave assisted treatment on the water vapor barrier properties of soybean  
537 protein isolate-based oleic acid/stearic acid blend edible films, *Food Hydrocoll.* 35 (2014)  
538 51–58. <https://doi.org/10.1016/j.foodhyd.2013.07.006>.
- 539 [13] M.C. Gómez-Guillén, M. Pérez-Mateos, J. Gómez-Estaca, E. López-Caballero, B. Giménez,  
540 P. Montero, Fish gelatin: a renewable material for developing active biodegradable films,  
541 *Trends Food Sci. Technol.* 20 (2009) 3–16. <https://doi.org/10.1016/j.tifs.2008.10.002>.
- 542 [14] H.M.C. Azeredo, M.F. Rosa, L.H.C. Mattoso, Nanocellulose in bio-based food packaging  
543 applications, *Ind. Crops Prod.* 97 (2017) 664–671.  
544 <https://doi.org/10.1016/j.indcrop.2016.03.013>.
- 545 [15] G. Siqueira, J. Bras, A. Dufresne, Cellulosic Bionanocomposites: A Review of Preparation,  
546 Properties and Applications, *Polymers (Basel)*. 2 (2010) 728–765.  
547 <https://doi.org/10.3390/polym2040728>.
- 548 [16] S.F. Hosseini, M.C. Gómez-Guillén, A state-of-the-art review on the elaboration of fish  
549 gelatin as bioactive packaging: Special emphasis on nanotechnology-based approaches,  
550 *Trends Food Sci. Technol.* 79 (2018) 125–135. <https://doi.org/10.1016/j.tifs.2018.07.022>.
- 551 [17] H.M.C. de Azeredo, Nanocomposites for food packaging applications, *Food Res. Int.* 42  
552 (2009) 1240–1253. <https://doi.org/10.1016/j.foodres.2009.03.019>.
- 553 [18] P. Squinca, S. Bilatto, A.C. Badino, C.S. Farinas, Nanocellulose production in future  
554 biorefineries: an integrated approach using tailor-made enzymes Nanocellulose production in  
555 future biorefineries : an integrated approach using tailor-made enzymes, *ACS Sustain. Chem.*  
556 *Eng.* 8 (2020) 2277–2286. <https://doi.org/10.1021/acssuschemeng.9b06790>.
- 557 [19] B. Thomas, M.C. Raj, K.B. Athira, M.H. Rubiyah, J. Joy, A. Moores, G.L. Drisko,  
558 Nanocellulose, a versatile green platform: from biosources to materials and their

- 559 applications, *Chem. Rev.* 118 (2018) 11575–11625.  
560 <https://doi.org/10.1021/acs.chemrev.7b00627>.
- 561 [20] R.J. Moon, G.T. Schueneman, J. Simonsen, Overview of Cellulose Nanomaterials, Their  
562 Capabilities and Applications, *Jom.* 68 (2016) 2383–2394. [https://doi.org/10.1007/s11837-](https://doi.org/10.1007/s11837-016-2018-7)  
563 016-2018-7.
- 564 [21] A. Dufresne, Polysaccharide nanocrystal reinforced nanocomposites, *Can. J. Chem.* 86  
565 (2008) 484–494. <https://doi.org/10.1139/V07-152>.
- 566 [22] C. Zhuang, F. Tao, Y. Cui, Eco-friendly biorefractory films of gelatin and TEMPO-oxidized  
567 cellulose ester for food packaging application, *J. Sci. Food Agric.* 97 (2017) 3384–3395.  
568 <https://doi.org/10.1002/jsfa.8189>.
- 569 [23] P. Sukyai, P. Anongjanya, N. Bunyahwuthakul, K. Kongsin, N. Harnkarnsujarit, U. Sukatta,  
570 R. Sothornvit, R. Chollakup, Effect of cellulose nanocrystals from sugarcane bagasse on  
571 whey protein isolate-based films, *Food Res. Int.* 107 (2018) 528–535.  
572 <https://doi.org/10.1016/j.foodres.2018.02.052>.
- 573 [24] J. George, Siddaramaiah, High performance edible nanocomposite films containing bacterial  
574 cellulose nanocrystals, *Carbohydr. Polym.* 87 (2012) 2031–2037.  
575 <https://doi.org/10.1016/j.carbpol.2011.10.019>.
- 576 [25] L.S.F. Leite, C.M. Ferreira, A.C. Corrêa, F.K.V. Moreira, L.H.C. Mattoso, Scaled-up  
577 production of gelatin-cellulose nanocrystal bionanocomposite films by continuous casting,  
578 *Carbohydr. Polym.* 238 (2020) 116198. <https://doi.org/10.1016/j.carbpol.2020.116198>.
- 579 [26] M. Le Gars, J. Bras, H. Salmi-Mani, M. Ji, D. Dragoe, H. Faraj, S. Domenek, N. Belgacem,  
580 P. Roger, Polymerization of glycidyl methacrylate from the surface of cellulose nanocrystals  
581 for the elaboration of PLA-based nanocomposites, *Carbohydr. Polym.* 234 (2020) 115899.  
582 <https://doi.org/10.1016/j.carbpol.2020.115899>.
- 583 [27] J. Tang, J. Sisler, N. Grishkewich, K.C. Tam, Functionalization of cellulose nanocrystals for

- 584 advanced applications, *J. Colloid Interface Sci.* 494 (2017) 397–409.  
585 <https://doi.org/10.1016/j.jcis.2017.01.077>.
- 586 [28] E. Espino-Pérez, J. Bras, G. Almeida, P. Relkin, N. Belgacem, C. Plessis, S. Domenek,  
587 Cellulose nanocrystal surface functionalization for the controlled sorption of water and  
588 organic vapours, *Cellulose*. 23 (2016) 2955–2970. <https://doi.org/10.1007/s10570-016-0994->  
589 [y](https://doi.org/10.1007/s10570-016-0994-y).
- 590 [29] H.W. Kwak, H. Lee, S. Park, M.E. Lee, H.-J. Jin, Chemical and physical reinforcement of  
591 hydrophilic gelatin film with di-aldehyde nanocellulose, *Int. J. Biol. Macromol.* 146 (2020)  
592 332–342. <https://doi.org/10.1016/j.ijbiomac.2019.12.254>.
- 593 [30] N.A. El-Wakil, E.A. Hassan, R.E. Abou-Zeid, A. Dufresne, Development of wheat  
594 gluten/nanocellulose/titanium dioxide nanocomposites for active food packaging, *Carbohydr.*  
595 *Polym.* 124 (2015) 337–346. <https://doi.org/10.1016/j.carbpol.2015.01.076>.
- 596 [31] F. V. Ferreira, M. Mariano, I.F. Pinheiro, E.M. Cazalini, D.H.S. Souza, L.S.S. Lapesqueur,  
597 C.Y. Koga-Ito, R.F. Gouveia, L.M.F. Lona, Cellulose nanocrystal-based poly(butylene  
598 adipate-co-terephthalate) nanocomposites covered with antimicrobial silver thin films,  
599 *Polym. Eng. Sci.* 59 (2019) pen.25066. <https://doi.org/10.1002/pen.25066>.
- 600 [32] R. Sharma, S.M. Jafari, S. Sharma, Antimicrobial bio-nanocomposites and their potential  
601 applications in food packaging, *Food Control*. 112 (2020) 107086.  
602 <https://doi.org/10.1016/j.foodcont.2020.107086>.
- 603 [33] Y. Zheng, K. Yao, J. Lee, D. Chandler, J. Wang, C. Wang, F. Chu, Well-defined renewable  
604 polymers derived from gum rosin, *Macromol. Commun. to Ed.* 43 (2010) 5922–5924.  
605 <https://doi.org/10.1021/ma101071p>.
- 606 [34] S. Kugler, P. Ossowicz, K. Malarczyk-Matusiak, E. Wierzbicka, Advances in rosin-based  
607 chemicals: The latest recipes, applications and future trends, *Molecules*. 24 (2019) 1651–  
608 1703. <https://doi.org/10.3390/molecules24091651>.

- 609 [35] X. Liu, W. Xin, J. Zhang, Rosin-based acid anhydrides as alternatives to petrochemical  
610 curing agents, *Green Chem.* 11 (2009) 1018–1025. <https://doi.org/10.1039/b903955d>.
- 611 [36] M. Narayanan, S. Loganathan, R.B. Valapa, S. Thomas, T.O. Varghese, UV protective  
612 poly(lactic acid)/rosin films for sustainable packaging, *Int. J. Biol. Macromol.* 99 (2017) 37–  
613 45. <https://doi.org/10.1016/j.ijbiomac.2017.01.152>.
- 614 [37] D.O. de Castro, J. Bras, A. Gandini, N. Belgacem, Surface grafting of cellulose nanocrystals  
615 with natural antimicrobial rosin mixture using a green process, *Carbohydr. Polym.* 137  
616 (2016) 1–8. <https://doi.org/10.1016/j.carbpol.2015.09.101>.
- 617 [38] F. Li, S.Y.H. Abdalkarim, H. Yu, J. Zhu, Y. Zhou, Y. Guan, Bifunctional Reinforcement of  
618 Green Biopolymer Packaging Nanocomposites with Natural Cellulose Nanocrystal–Rosin  
619 Hybrids, *ACS Appl. Bio Mater.* 3 (2020) 1944–1954.  
620 <https://doi.org/10.1021/acsabm.9b01100>.
- 621 [39] X. Niu, Y. Liu, Y. Song, J. Han, H. Pan, Rosin modified cellulose nanofiber as a reinforcing  
622 and co-antimicrobial agents in polylactic acid/chitosan composite film for food packaging,  
623 *Carbohydr. Polym.* 183 (2018) 102–109. <https://doi.org/10.1016/j.carbpol.2017.11.079>.
- 624 [40] E. Espino-Pérez, S. Domenek, N. Belgacem, C. Sillard, J. Bras, Green Process for Chemical  
625 Functionalization of Nanocellulose with Carboxylic Acids, *Biomacromolecules.* 15 (2014)  
626 4551–4560. <https://doi.org/10.1021/bm5013458>.
- 627 [41] L. Segal, J.J. Creely, A.E. Martin, M. Conrad, An Empirical Method for Estimating the  
628 Degree of Crystallinity of Native Cellulose Using the X-Ray Diffractometer, *Text. Res. J.* 29  
629 (1959) 786–794.
- 630 [42] N. Paudyal, V. Anihouvi, J. Hounhouigan, M. Ignatius, B. Sekwati-monang, W. Amoa-awua,  
631 A. Atter, N. Bernice, S. Mbugua, A. Asagbra, W. Abdelgadir, J. Nakavuma, M. Jakobsen, W.  
632 Fang, Microbiology prevalence of foodborne pathogens in food from selected African  
633 countries – a meta-analysis, *Int. J. Food Microbiol.* 249 (2017) 35–43.

- 634 <https://doi.org/10.1016/j.ijfoodmicro.2017.03.002>.
- 635 [43] C. Ferrario, G. Andrea, M. Cristina, F. Turrone, C. Milani, S. Duranti, L. Mancabelli, M.  
636 Mangifesta, G. Alessandri, D. Van Sinderen, M. Ventura, Microbiology next generation  
637 sequencing-based multigene panel for high throughput detection of food-borne pathogens,  
638 *Int. J. Food Microbiol.* 256 (2017) 20–29. <https://doi.org/10.1016/j.ijfoodmicro.2017.05.001>.
- 639 [44] E. hadji B. Ly, J. Bras, P. Sadocco, M.N. Belgacem, A. Dufresne, W. Thielemans, Surface  
640 functionalization of cellulose by grafting oligoether chains, *Mater. Chem. Phys.* 120 (2010)  
641 438–445. <https://doi.org/10.1016/j.matchemphys.2009.11.032>.
- 642 [45] L.S.F. Leite, L.C. Battirola, L.C.E. da Silva, M. do C. Gonçalves, Morphological  
643 investigation of cellulose acetate/cellulose nanocrystal composites obtained by melt  
644 extrusion, *J. Appl. Polym. Sci.* 133 (2016) 1–10. <https://doi.org/10.1002/app.44201>.
- 645 [46] R.F. Vázquez, M.A. Daza Millone, F.J. Pavinatto, V.S. Herlax, L.S. Bakás, O.N. Oliveira,  
646 M.E. Vela, S.M. Maté, Interaction of acylated and unacylated forms of *E. coli* alpha-  
647 hemolysin with lipid monolayers: a PM-IRRAS study, *Colloids Surfaces B Biointerfaces.*  
648 158 (2017) 76–83. <https://doi.org/10.1016/j.colsurfb.2017.06.020>.
- 649 [47] F. Severcan, P.I. Haris, *Vibrational Spectroscopy in Diagnosis and Screening*, 1 edition, IOS  
650 Press, Amsterdam, 2012.
- 651 [48] B. Więckowski, A., Korzeniewski, C., Braunschweig, *Vibrational spectroscopy at electrified*  
652 *interfaces*, John Wiley & Sons, Inc., Hoboken, NJ, USA, 2013.  
653 <https://doi.org/10.1002/9781118658871>.
- 654 [49] N.B. Coltrup, L.H. Daly, S.E. Wiberley, *Introduction to infrared and raman spectroscopy*, 3rd  
655 editio, Elsevier, Boston, 1990. <https://doi.org/10.1016/B978-0-12-182552-2.X5001-3>.
- 656 [50] K. Chuaynukul, M. Nagarajan, T. Prodpran, S. Benjakul, P. Songtipya, L. Songtipya,  
657 *Comparative Characterization of Bovine and Fish Gelatin Films Fabricated by Compression*  
658 *Molding and Solution Casting Methods*, *J. Polym. Environ.* 26 (2018) 1239–1252.

- 659 <https://doi.org/10.1007/s10924-017-1030-5>.
- 660 [51] Ó.L. Ramos, J.C. Fernandes, S.I. Silva, M.E. Pintado, F.X. Malcata, Edible Films and  
661 Coatings from Whey Proteins: A Review on Formulation, and on Mechanical and Bioactive  
662 Properties, *Crit. Rev. Food Sci. Nutr.* 52 (2012) 533–552.  
663 <https://doi.org/10.1080/10408398.2010.500528>.
- 664 [52] J.-W. Rhim, H.-M. Park, C.-S. Ha, Bio-nanocomposites for food packaging applications,  
665 *Prog. Polym. Sci.* 38 (2013) 1629–1652. <https://doi.org/10.1016/j.progpolymsci.2013.05.008>.
- 666 [53] S.Y. Ooi, I. Ahmad, M.C.I.M. Amin, Cellulose nanocrystals extracted from rice husks as a  
667 reinforcing material in gelatin hydrogels for use in controlled drug delivery systems, *Ind.*  
668 *Crops Prod.* 93 (2016) 227–234. <https://doi.org/10.1016/j.indcrop.2015.11.082>.
- 669 [54] T.M. Santos, M.D.S.M. Souza Filho, C.A. Caceres, M.F. Rosa, J.P.S. Morais, A.M.B. Pinto,  
670 H.M.C. Azeredo, Fish gelatin films as affected by cellulose whiskers and sonication, *Food*  
671 *Hydrocoll.* 41 (2014) 113–118. <https://doi.org/10.1016/j.foodhyd.2014.04.001>.
- 672 [55] M.R.E. Santos, A.C. Fonseca, P. V. Mendonça, R. Branco, A.C. Serra, P. V. Morais, J.F.J.  
673 Coelho, Recent developments in antimicrobial polymers: A review, *Materials (Basel)*. 9  
674 (2016). <https://doi.org/10.3390/MA9070599>.
- 675 [56] M. Ahmad, S. Benjakul, T. Prodpran, T.W. Agustini, Physico-mechanical and antimicrobial  
676 properties of gelatin film from the skin of unicorn leatherjacket incorporated with essential  
677 oils, *Food Hydrocoll.* 28 (2012) 189–199. <https://doi.org/10.1016/j.foodhyd.2011.12.003>.
- 678 [57] J. Wang, Y.P. Chen, K. Yao, P.A. Wilbon, W. Zhang, L. Ren, J. Zhou, M. Nagarkatti, C.  
679 Wang, F. Chu, X. He, A.W. Decho, C. Tang, Robust antimicrobial compounds and polymers  
680 derived from natural resin acids, *Chem. Commun.* 48 (2012) 916–918.  
681 <https://doi.org/10.1039/c1cc16432e>.
- 682 [58] A. Cagri, Z. Ustunol, E.T. Ryser, Antimicrobial, mechanical, and moisture barrier properties  
683 of low pH whey protein-based edible films containing p-aminobenzoic or sorbic acids, *J.*

684 Food Sci. 66 (2001) 865–870. <https://doi.org/10.1111/j.1365-2621.2001.tb15188.x>.

685

## Eco-friendly gelatin films reinforced with rosin-grafted cellulose nanocrystals for antimicrobial packaging applications

Liliane S. F. Leite<sup>a,b,c</sup>, Stanley Bilatto<sup>b</sup>, Rafaella T. Paschoalin<sup>c</sup>, Andrey C. Soares<sup>b</sup>, Francys K. V. Moreira<sup>d</sup>, Osvaldo N. Oliveira Jr.<sup>c</sup>, Luiz H. C. Mattoso<sup>a,b</sup>, Julien Bras<sup>e</sup>

Fig. 1. C<sub>1s</sub> XPS spectra of (a) CNCs and (b) r-CNCs. (c) ATR-FTIR spectra of rosin, CNCs, and r-CNCs. (d) TEM micrograph of CNCs and (e) r-CNCs. (f) schematic representation of rosin-functionalized CNCs.

Fig. 2. SEM micrographs of the cross-sectional surface of (a) pure gelatin films and gelatin bionanocomposites with 4.0 wt% (b) CNCs and (c) r-CNCs, and with 6.0 wt% (d) CNCs and (e) r-CNCs content.

Fig. 3: PM-IRRAS spectra of gelatin film and gelatin bionanocomposites with 6 wt% CNCs and 6 wt% r-CNCs. The spectrum of a clean gold substrate was used as a baseline.

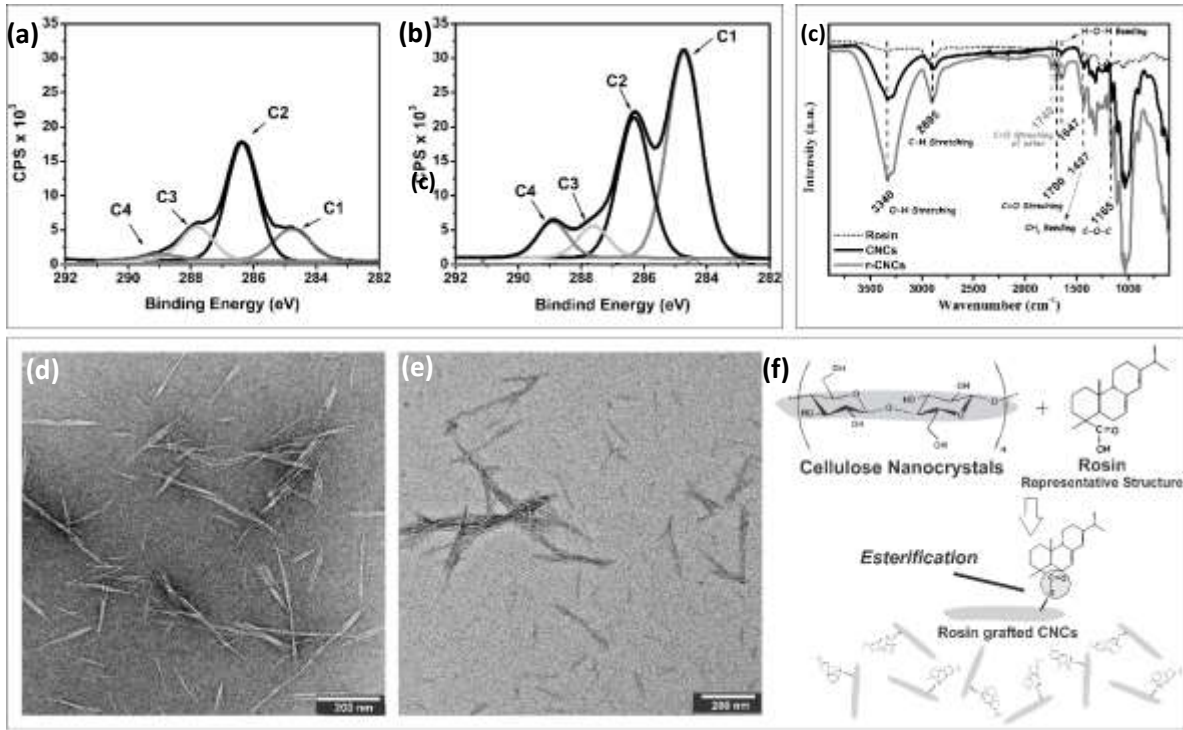
Fig. 4. Photography of (a) gelatin/CNCs and (b) gelatin/r-CNCs bionanocomposite films.

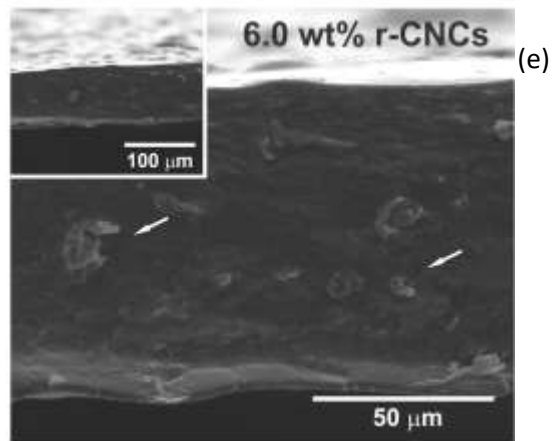
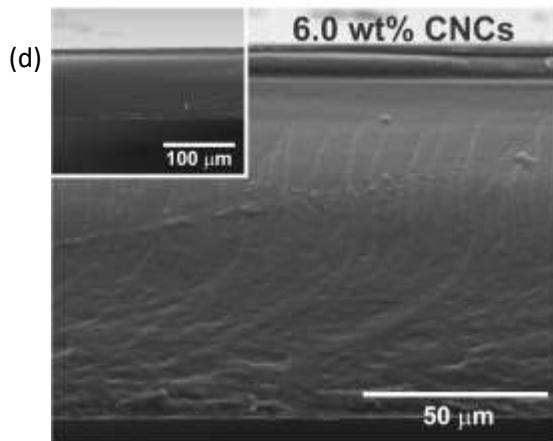
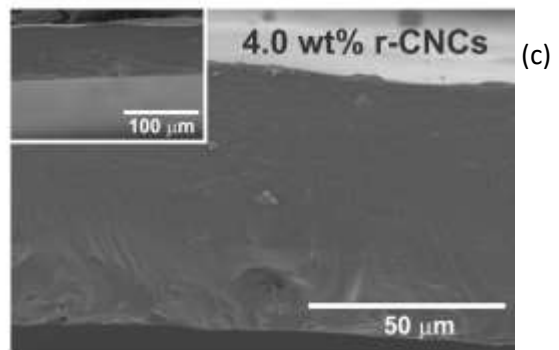
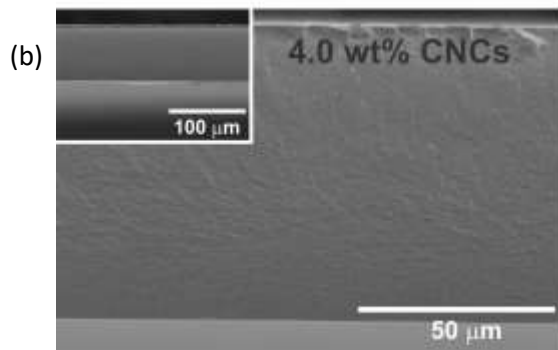
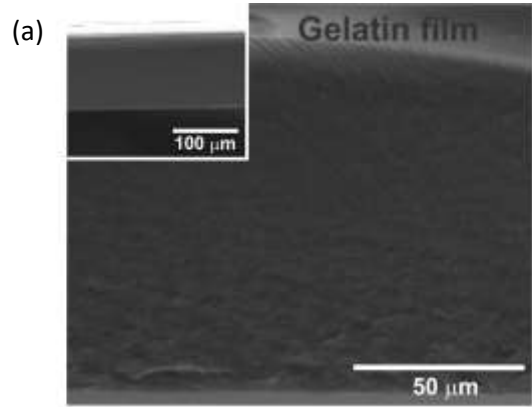
Fig. 5. (a) Young's modulus, (b) tensile strength (c) elongation at break, and (d) stress-strain curves as a function of CNCs and r-CNCs content in bionanocomposite gelatin films obtained by casting.

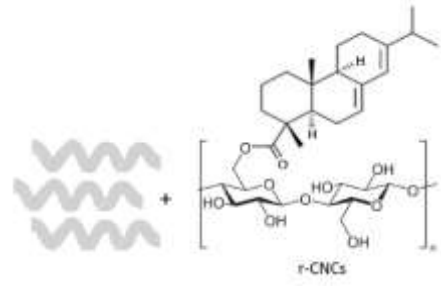
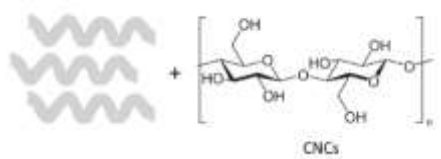
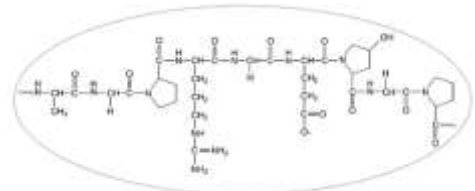
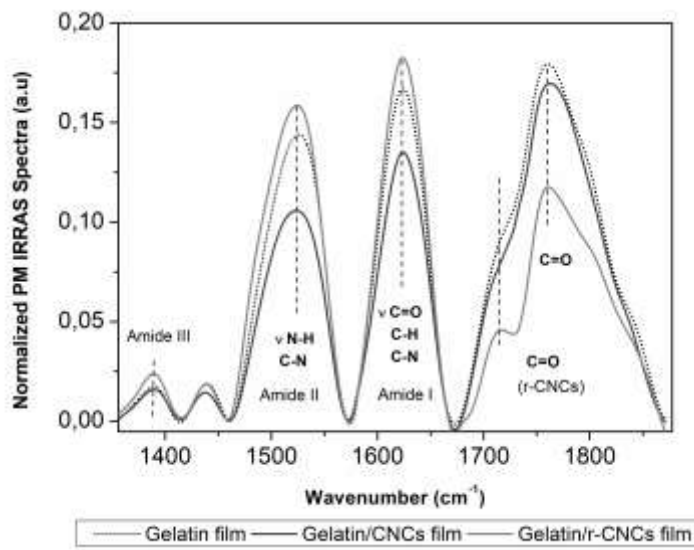
Fig. 6. Minimum inhibitory concentration (MIC) of CNCs and r-CNCs suspension tested on Gram-positive *Staphylococcus aureus* and Gram-negative *Escherichia coli*.

Fig. 7. Agar overlay assay of gelatin film discs against *S. aureus* and *E. coli*.

Fig. 8: Schematic comparison of accelerated storage for mozzarella cheese slices packed in a PVC cling film, pure gelatin film, and gelatin/r-CNCs nanocomposite (6 wt%) film over 30 days at 25 °C. The control refers to free-standing, unpacked cheese slices (The Brazilian version of mozzarella cheese can be sliced, in contrast to the Italian mozzarella). Microbial spoilage is indicated by arrows in the images.

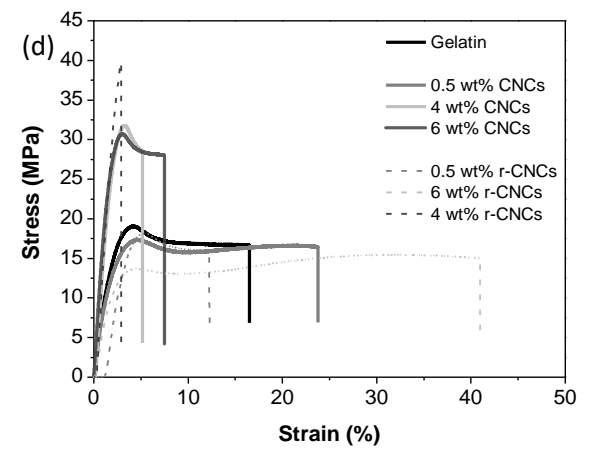
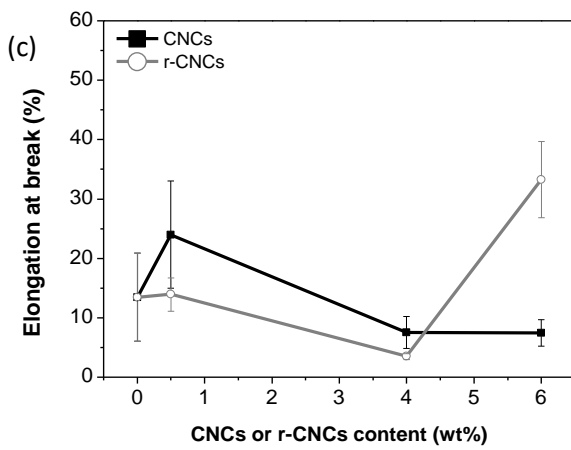
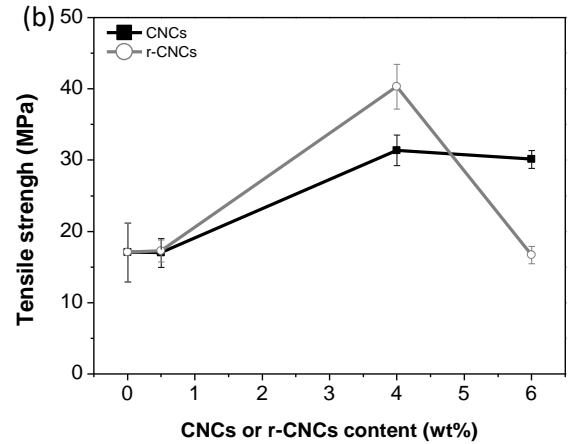
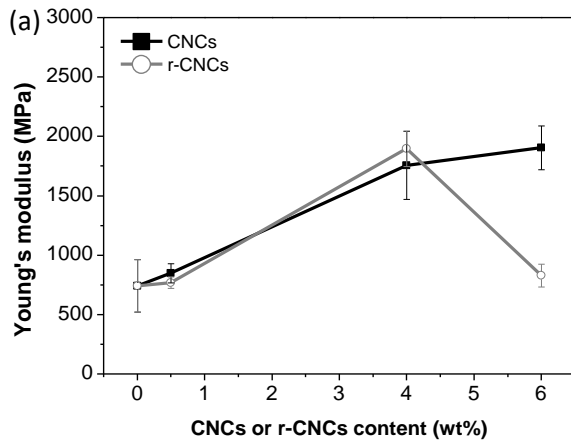




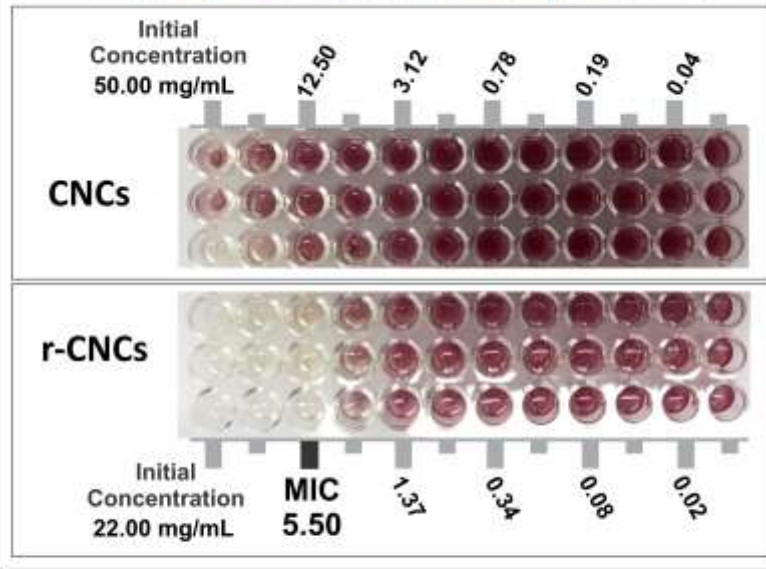


\*Representative formulas

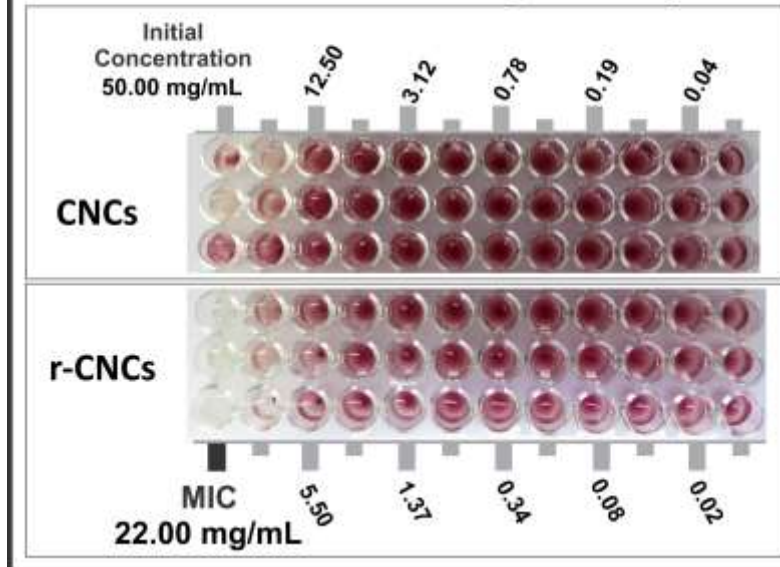




### *Staphylococcus aureus* (Gram +)



### *Escherichia coli* (Gram -)





*E. coli* - gelatin/CNCs



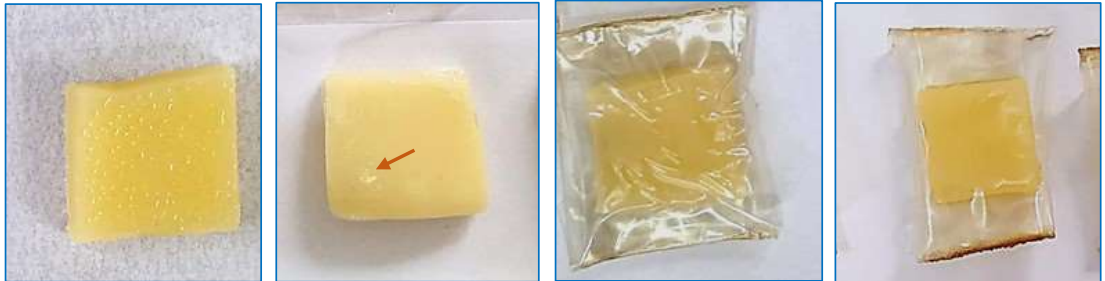
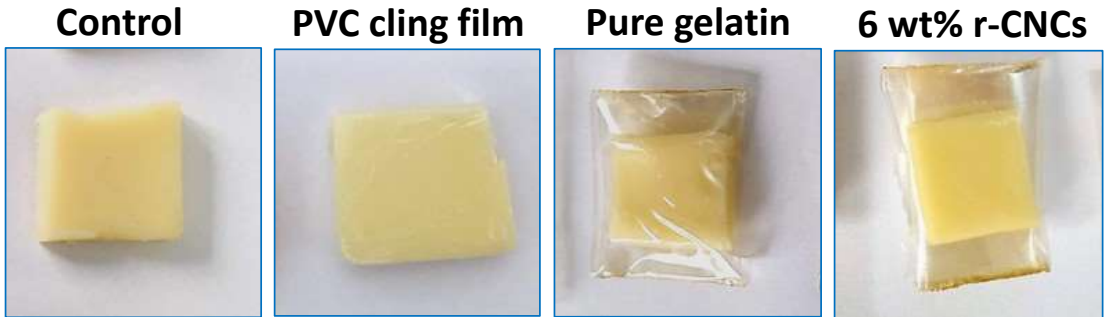
*E. coli* - gelatin/r-CNCs



*S. aureus* - gelatin/CNCs



*S. aureus* - gelatin/r-CNCs



## Eco-friendly gelatin films reinforced with rosin-grafted cellulose nanocrystals for antimicrobial packaging applications

*Liliane S. F. Leite<sup>a,b,c</sup>, Stanley Bilatto<sup>b</sup>, Rafaella T. Paschoalin<sup>c</sup>, Andrey C. Soares<sup>b</sup>, Francys K. V. Moreira<sup>d</sup>, Osvaldo N. Oliveira Jr.<sup>c</sup>, Luiz H. C. Mattoso<sup>a,b</sup>, Julien Bras<sup>e</sup>*

Table 1: X-ray photoelectron spectroscopy data of CNCs and r- CNCs

Cellulose nanoparticles	O/C	Binding energy, eV			
		C1: C-C 285.0	C2: C-O 286.6	C3: O-C-O 288.0	C4: O=C-O 289.1
CNCs	0.61	16.4	62.6	17.2	3.8
r-CNCs	0.33	52.1	32.5	7.3	8.1

Table 2: optical properties of gelatin/r-CNCs bionanocomposite and synthetic films currently applied in food packaging.

Film	Light transmission (%)			
	200 nm	280 nm	400 nm	600 nm
0.5 wt% gelatin/r-CNCs	0.0	4.5	77.3	87.4
6.0 wt% gelatin/r-CNCs	0.0	5.4	60.5	66.7
Synthetic films currently applied in food packaging <sup>a</sup>				
LDPE <sup>a</sup>	13.1	67.5	83.4	86.9
OPP <sup>a</sup>	4.6	80.0	87.9	89.1
PVC	20	83.9	87.9	88.7

LDPE: low-density polyethylene; OPP: oriented polypropylene; PVC: polyvinyl chloride

<sup>a</sup> adapted from [50].